

Numerical Modeling of Compliant-Moored System Dynamics with
Applications to Marine Energy Converters

Tyler Nichol

A thesis
submitted in partial fulfillment of the
requirements for the degree of

Master of Science in Mechanical Engineering

University of Washington

2014

Committee:

Brian Fabien, Chair

Brian Polagye

Jim Thomson

Program Authorized to Offer Degree:

Department of Mechanical Engineering

©Copyright 2014
Tyler Nichol

University of Washington

Abstract

Numerical Modeling of Compliant-Moored System Dynamics with
Applications to Marine Energy Converters

Tyler Nichol

Chair of the Supervisory Committee:
Professor Brian Fabien
Mechanical Engineering

The development of a numerical model simulating the dynamic response of compliant-moored submerged systems to non-uniform fluid flow is presented. The model is meant to serve as a computational tool with applications to compliant-moored marine energy converters by time-domain representation of the mooring dynamics. The scope of the initial code is restricted to full-submerged moored tidal turbines, though the model can be readily expanded to analyze wave energy converters as well. The system is modeled in a Lagrangian frame treating tidal turbines and structural elements as rigid bodies. Mooring lines are modeled as a series of discrete elastic segments, with parameters and force contributions lumped to point-mass nodes joining each segment. Full-range of motion is achieved using the α - β - γ Euler Angle method. The governing equations of motion of the system are derived computationally through implementation of Lagrange's Equation of Motion. The techniques employed to develop the symbolic expressions for the total kinetic, potential, and damping energies of the system and the forces acting on each element of the system are discussed. The system of differential equations obtained from evaluation of Lagrange's Equation with the developed symbolic expressions is solved numerically using a built-in MATLAB ordinary differential equation solver called *ODE15i.m* with the user defined initial condition of the system. Several validation tests are presented and their results discussed. Finally, an explanation of future plans for development of the model and application to existing tidal energy systems are presented.

Acknowledgements

I would like to thank my research advisor, Professor Brian Fabien. Your support and encouragement throughout this project has been greatly appreciated. I would also like to thank the other two members of my supervisory committee, Professors Brian Polagye and Jim Thomson, both of whom have helped advance my understanding of tidal energy systems through their support of this project. I wish to acknowledge the financial support of the US Department of Energy under DE-FG36-08GO18179-M001. Finally, I would like to express my gratitude to the Northwest National Marine Renewable Energy Center for the opportunity to get involved in the fascinating field of marine renewable energy.

Table of Contents

1. Introduction.....	1
2. Background on Tidal Energy and Numerical Methods.....	3
2.1. Moored tidal turbine projects.....	5
2.2. Commercially available software	7
3. System Model Description	9
3.1. Fluid flow characteristics.....	10
3.2. Device Configuration	11
3.2.1. Rigid bodies	14
3.2.2. Mooring lines.....	14
3.3. Kinematics	15
3.3.1. Rigid Body Euler Angles	17
3.3.2. Line discretization.....	21
3.4. Lagrange’s Equation of Motion.....	21
3.5. Kinetic Energy	22
3.6. Potential Energy.....	26
3.7. Rate of Energy Dissipation.....	27
3.8. Force Contributors.....	28
3.8.1. Gravity.....	29
3.8.2. Buoyancy	31
3.8.3. Fluid Forces	32
3.8.3.1. Drag and lift.....	33
3.8.3.2. Added mass.....	38
3.8.3.3. Vortex-induced motion	39
3.8.4. Seafloor Impenetrability.....	40
3.8.5. Applied Forces.....	41
3.9. Numerical Solution	41

4. Model Validation	42
4.1. Steady State Systems	42
4.1.1. Elastic catenary.....	42
4.1.2. Point-mass on line with fixed end points.....	46
4.1.3. Comparison to Steady-State Tidal Turbine Equilibrium Model.....	49
4.2. Dynamic Systems	52
4.2.1. Mass-Spring-Damper system.....	53
5. Future work	56
5.1. Turbulence Modelling and Dynamic Comparison	57
5.1.1. Dynamic Comparison to TTM Deployment.....	58
5.2. Initialize to equilibrium	59
5.3. Collaboration.....	60
6. Conclusion	61
7. References.....	63
Appendix A. How to use UWMooringDynamics.m	65
A.1. Setting General System Parameters	65
A.2. Adding Rigid Bodies	68
A.3. Adding Free Nodes	71
A.4. Adding Mooring Lines.....	71
A.5. Example: DuBuque System.....	73
Appendix B. UWMooringDynamics program files	77

List of Figures

Figure 1: Andritz Hydro Hammerfest HS1000 Tidal Turbine [5]	4
Figure 2: MCT Ltd. SeaGen Tidal Energy Device	5
Figure 3: Schematic of Single-Point Tensioned Contra Rotating Tidal Turbine (CoRMaT) [11]	6
Figure 4: Rendering of Ocean Renewable Power Company's OCGen Power System [12]	6
Figure 5: Simple Single Turbine System	12
Figure 6: Single point tensioned tidal turbine featuring one free node	12
Figure 7: Tidal turbine system featuring one free turbine and one constrained turbine.....	13
Figure 8: Rigid Body Kinematic System	15
Figure 9: Line Segment Kinematic System	16
Figure 10: Euler Angle Coordinate Transformation	17
Figure 11: Component-wise drag calculation for rigid body.....	33
Figure 12: Drag Calculation for Line Segment.....	36
Figure 13: Elastic catenary benchmark test geometry	42
Figure 14: Elastic Catenary – Numerical solution (black line with data points indicated by 'o') overlaid on analytical solution (red curve).....	45
Figure 15: Maximum error of numerical solution as a function of increasing number of line segments .	45
Figure 16: Point mass on line with fixed end points	46
Figure 17: Fixed end-points with single point-mass – Numerical solution (black line with data points indicated by 'o') overlaid on analytical solution (red curve).....	48
Figure 18: System schematic for comparison to static-equilibrium model	49
Figure 19: Static-equilibrium obtained from dynamic model.....	52
Figure 20: Equilibrium position obtained from static model [26].....	52
Figure 21: Mass-Spring-Damper system for first dynamic validation test.....	54
Figure 22: Error as a function of ODE Solver tolerances.....	56
Figure 23: Tidal Turbulence Mooring data collection instrument	58
Figure 24: Acceleration Spectra of TTM response to turbulent flow [17]	59
Figure 25: UNH barge-mounted hydrokinetic turbine [27]	60
Figure 26: Measured response of barge to fluid loading compared to UNH predictions.....	61
Figure 27: Default animation space and viewing angle	67

List of Tables

Table 1: Static comparison benchmark test - Rigid body properties.....	50
Table 2: Static comparison benchmark test – Mooring line properties	51
Table 3: Static comparison benchmark test - Results.....	51
Table 4: Default values for general system parameters	66
Table 5: Parameters and default values associated with rigid bodies.....	68
Table 6: Parameters and default values associated with mooring lines.....	72

1. Introduction

As the world's energy demands continue to rise and the effects of climate change become more apparent, it is clear that we as a society must continue to look for new and innovative sources of energy that do not emit harmful greenhouse gasses into the atmosphere. Tremendous progress has been over the past 40 years in the field of wind power, and that technology is currently being used across the globe to generate clean, sustainable energy. According to the U.S. Energy Information Administration, wind power was used to generate roughly 1.7% of all electricity consumed worldwide in 2010 [1]. Though this is only a small fraction of the total power produced, it is not for lack of effective engineering solutions for capturing wind energy, but rather it is due to social, political, and economic roadblocks which are only slowly being cleared away. Some countries, such as Denmark, have managed to employ wind power technologies to generate up to 20% of their total energy demand [1].

It took many years and the diligent efforts of innumerable researchers to develop wind energy into a viable technology, and now the same efforts are needed to grow other industries in hopes of increasing the portion of energy that can be generated by environmentally sound and sustainable means. One of these industries focuses on marine energy, wherein the power of ocean waves and tidal currents are captured and converted into electricity for human consumption. These emerging technologies have a long way to go before achieving the widespread success of the wind industry, but as continued research reveals new and effective methods for capturing marine energy in a responsible manner, it moves closer and closer to becoming a viable method for clean and sustainable energy generation.

Tidal energy, a component of the greater marine renewable energy field, harnesses the kinetic energy in tidally driven ocean currents for electricity generation. As gravitational forces from the sun and moon cause the ocean surface to rise and fall, water flows through the relatively narrow inlets to bays, sounds, sea lochs, or other geological features, creating an appreciable current. By placing a turbine in those flows, a generator can be turned to create electricity. Tidal turbines are analogous to wind turbines in

that a fluid flow past the turbine blades generates lift, causing the blades to rotate about a hub, the shaft of which is connected to the rotor of an electric generator.

Though the idea of tidal energy generation is simple in principle, it is much more difficult in execution. Issues arise as a result of the very nature of placing mechanical devices in the harsh marine environment, where corrosion and bio-fouling place limits on the useful life of such devices, and where installing any structure to earth submerged in up to hundreds of meters of seawater requires a tremendous engineering effort. Most designs for tidal turbines incorporate a rigid mounting structure which is either pile-driven into the seabed [2] or is designed such that gravitational forces keep the structure upright when subjected to high currents [3]. Pile-supported turbines are typically feasible in water depths up to 40 *m*. Gravity foundations may be deployed in deep water, but the foundation weight required to resist overturning limits hub heights to the less energetic portion of the water column, limiting the output power of the device.

A mooring concept that combines the ease of deployment of gravity foundations with the advantageous hub heights of pile foundations is to design buoyancy into the turbine and anchor it to the sea floor via flexible mooring lines. Compliant-moored turbines would introduce fewer environmental stressors, given the small area of disturbed seabed and limited amount of hard substrate introduced into marine environments [4]. Additionally, this method has the advantage of allowing turbines to be deployed in deep water, since the turbines can operate in the more energetic flows occurring higher in the water column without inducing an overturning moment onto the support structure. To assist in the design of single or arrays of compliant-moored tidal turbines, we have developed a software tool to simulate mooring performance. This consists of a numerical simulation implemented in MATLAB (www.mathworks.com) of a moored turbine system that, when given the necessary input parameters, models the dynamic response of the mooring system to a specified flow field. This information will help turbine developers determine the best configuration of turbines and mooring lines to maintain the

optimal turbine orientation to the fluid flow and position in the water column while staying within structural loading limits. Furthermore, this tool will be helpful in the design of active or passive control systems to optimize turbine position, as the performance of various control techniques and parameters can be evaluated computationally, reducing the overall effort and expense associated with field testing. The methods described herein were developed primarily with consideration to moored tidal turbines, though they will eventually be expanded to include effects of surface waves and could thus also be applied to wave energy converters or offshore wind platforms.

The work presented herein discusses the development of this compliant-moored turbine modelling tool. A detailed description of the system is provided that comprehensively considers the forces acting on the system and explains how each component is modelled. Following this is an explanation of how the governing equations of motion for the system are obtained using Lagrange's equation of motion. Next, a number of validating test cases comparing the results of simple systems modeled using these methods to either analytical solutions or experimental data are presented. Ideas and plans for future development and implementation of these methods are then discussed. A user's guide explaining how to set up a model in the program and how to implement the tools developed as part of this project is offered in the Appendix.

2. Background on Tidal Energy and Numerical Methods

Because the principles of tidal energy closely resemble those of wind energy, many designs are heavily influenced by successes in the wind industry. Some devices, such as the 1 MW Andritz Hydro Hammerfest HS1000 shown in Figure 1, appear very much like underwater wind turbines. The HS1000 is being installed in an array consisting of 10 turbines for demonstration purposes in the Sound of Islay off the west coast of Scotland [5].

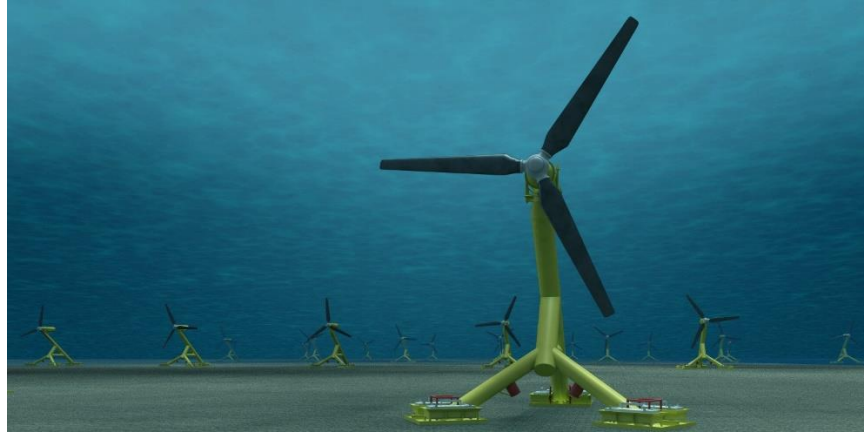


Figure 1: Andritz Hydro Hammerfest HS1000 Tidal Turbine [5]

Due to the analogies between wind and tidal energy harvesting, the three-bladed turbine design mounted to a tall, rigid support structure commonly seen in commercial scale wind energy projects is a reasonable starting point for tidal turbine research and development. However, as more data related to the deployment and operation of these devices accumulates, their limitations and the factors affecting performance become better understood, and new designs are developed to address these issues. This can be seen in the design of the SeaGen tidal stream generator developed by Marine Current Turbines Ltd (MTC), shown in Figure 2. Because of the difficulty in servicing any device while it is underwater, performing maintenance on a tidal energy device poses a challenge. The costs associated with recovering a device from its support structure to perform routine maintenance can be prohibitive. In an effort to facilitate maintenance operations, MTC developed a platform for a pair of tidal turbines that can be hydraulically lifted to a position above the surface of the water, significantly reducing the costs for maintenance and repair of the turbines.

This solution is suitable for tidal energy sites with relatively shallow depths and the SeaGen tidal energy device is currently operating for testing purposes in 24 meters of seawater in the Strangford Lough in the Northeast corner of Northern Ireland [6]. Commercial deployment projects are currently underway with plans to install an array of 9 devices off the coast of Anglesey in Wales, UK, at a depths ranging

from 20 to 40 meters [7]. To deploy this technology at greater depths would necessitate a significantly larger construction effort to ensure the monopole structure is able to withstand the increased moment that results from fluid drag forces acting at farther distances from the root. The costs associated with the added construction demand for installation in deep water limit the allowable deployment site depth to roughly 40 meters [8].

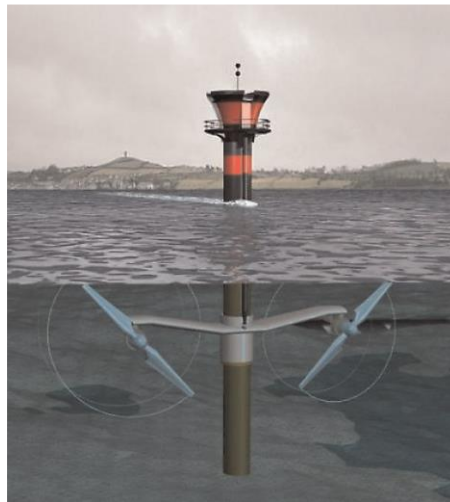


Figure 2: MCT Ltd. SeaGen Tidal Energy Device

2.1. Moored tidal turbine projects

Within the growing field of tidal energy harvesting, compliant moored devices have often been mentioned as a potential area for investigation to address difficulties associated with deep water tidal turbine deployment and recovery and to alleviate some of the environmental concerns that go with installing large structures of hard substrate to the marine environment [3,9,10]. The Energy Systems Research Unit (ESRU) at the University of Strathclyde is developing a device that employs a single mooring line anchored to the sea floor and tensioned using a buoy that may or may not be surface-penetrating, with a neutrally buoyant tidal turbine attached to the line at some point along its length [11]. The turbine features two sets of blades rotating in opposite directions to eliminate the reactive torque that occurs from a single set of turbine blades. A schematic of their contra-rotating tidal turbine,

dubbed CoRMaT, is shown in Figure 3. This device has undergone successful testing at sea in an energetic ocean current and ESRU is currently working on up-scaling and long-term reliability testing of the device.

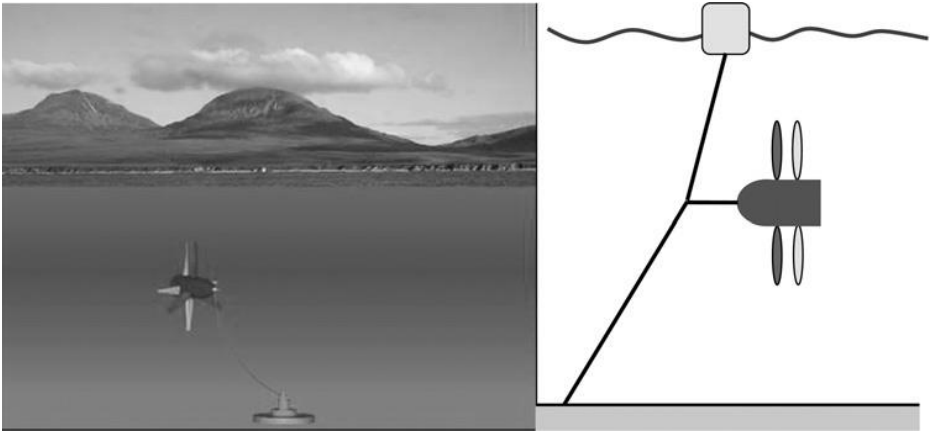


Figure 3: Schematic of Single-Point Tensioned Contra Rotating Tidal Turbine (CoRMaT) [11]

A second project is being led by Ocean Renewable Power Company (ORPC). The device, named the OCGen Power System, consists of an array of helical cross-flow turbines which resemble vertical axis wind turbines. A rendering of this device is given in Figure 4. The turbines are held in place on the seafloor by a system of mooring lines. Because of the reduced construction effort required to anchor the mooring lines as compared to installing rigid support structures in the seafloor, the OCGen is intended for deployment in water depths surpassing 80 meters with relatively low environmental impact [12].

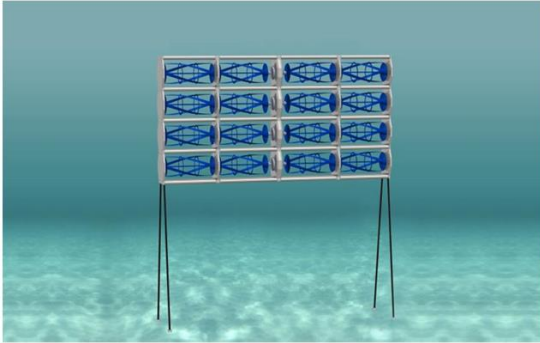


Figure 4: Rendering of Ocean Renewable Power Company's OCGen Power System [12]

2.2. Commercially available software

The development of compliant-moored tidal turbine systems could be well supported by a time-domain dynamic model. Clark et al. [11] discuss the importance of predicting instabilities in a compliant-moored system to achieve optimal performance. An accurate model of the mooring dynamics of a system has the potential to reveal flow conditions that result in oscillatory resonant behavior or instabilities that may not be expected without a comprehensive model of the system. Different mechanisms for eliminating or compensating for instabilities can also be evaluated using an accurate dynamic model before experimental methods are employed, thereby allowing a wide range of options to be investigated in a relatively short period of time and using minimal resources.

There are currently several options for software packages capable of performing dynamic analysis on moored tidal energy systems. One of these is OrcaFlex (www.orcina.com), a time-domain numerical solver which is widely used in many marine engineering industries to perform dynamic analysis of offshore marine systems. OrcaFlex was used by Columbia Power Technologies, LLC (CPT), to aid in the design of a wave energy converter [13]. The program was employed to evaluate significant design changes to the device in terms of performance in a relatively low-cost and low-impact manner. They found that, due to the specific nature of ocean energy harvesting devices, off-the-shelf software packages often need to be supplemented with custom-made numerical approaches [13]. To accurately model the system, CPT worked with Garrad Hassan and Partners (GH) to develop a numerical modelling package suited to their applications. Through implementation of the GH Wavefarmer software to examine frequency-domain behavior, and importing terms obtained from the frequency-domain modelling into OrcaFlex, they were able to generate a model for the mooring behavior of a WEC which closely resembled experimental results from data collected from a 1/33 scale test device [13].

Another fully dynamic, time-domain hydrodynamic simulator was developed by Dynamic Systems Analysis, Ltd. ProteusDS (www.dsa-ltd.ca) specializes in underwater cable dynamics and can model systems consisting of both rigid bodies and flexible cables and nets by employing finite-element discretization of flexible members and a nonlinear hydrodynamic cable model. This program was used by Hall et al. [14] to model the dynamic behavior of floating offshore wind turbines through coupling with a quasi-static aero-hydro simulator called FAST (wind.nrel.gov/designcodes/simulators/fast), which uses Blade-Element-Momentum Theory and linear hydrodynamics to describe a floating wind turbine device [15]. In addition, FAST includes a quasi-static model of taut or slack mooring lines by solving a system of analytical catenary cable equations to find the static-equilibrium position and tension of the lines. The linear hydrodynamics simulator WAMIT (www.wamit.com) was used to model the hydrodynamic loads on the floating wind turbine platform. Coupling of FAST with ProteusDS yields a fully dynamic finite element model of floating wind turbine system dynamics. The static-equivalent results from the dynamic model of a floating offshore wind turbine were compared to results found using FAST's default quasi-static mooring model, and the two were found to be in good agreement [14]. Further testing involving irregular sea states that cause the motions of the floating platform and surface waves to be out of sync will reveal a more complete picture of the differences between the fully-dynamic model and the quasi-static model.

Though these software packages exist and have been shown to be applicable to several marine energy systems with good accuracy, the development of a new computational tool from first-principles is justified by the following: 1) Code can be developed for specific functionalities and readily expanded to include secondary effects or to accept different formats of system parameter inputs (for example, one might express fluid velocity as a function of time and space or as a velocity vector field). 2) Due to the wide range of systems that commercial packages can model, creating even simple models can be cumbersome. This makes them less suitable as a rapid-iteration design tool for mooring arrangements

when many different configurations may need to be examined. Developing code for particular application to compliant-moored systems enables new models to be constructed using simple commands and in a relatively shorter time, allowing for more configurations to be evaluated. 3) Complete control over both how the model is constructed and how the solution is obtained allows for greater confidence in the results. 4) Greater flexibility when integrating with other computational tools such as active system control methods. This model can also be incorporated into commercial codes to provide details about the dynamic behavior of a mooring arrangement that is part of a larger system. It is also believed that having the experience of writing a proprietary program to model the system dynamics of compliant-moored tidal turbines will yield long term educational benefits to the National Northwest Marine Renewable Energy Center by enhancing the collective knowledge of moored tidal turbine system characteristics and modeling practices.

3. System Model Description

This section explains the scope of systems that can be analyzed and the methods adopted to describe the system mathematically for use by the computational tool developed herein. The techniques used to model all aspects of the system such as the mooring line dynamic characteristics and the fluid forces applied to the system are presented in detail.

The notation used to define vector quantities throughout this section and the rest of this document is shown below. The superscript leading the vector name indicates the coordinate frame in which the vector is expressed. The leading subscript identifies the type of system feature with which the vector is associated, which can be a free body (*B*), constrained body (*CB*), free node (*FN*), mooring line node (*LN*), or mooring line segment (*LS*). The trailing subscript indicates the specific feature number.

$$\overset{Frame}{Type} \overrightarrow{Vector}_{No.}$$

For example, the velocity of body i expressed as a vector with respect to the body-fixed frame j is ${}^j_B\vec{V}_i$.

The inertial coordinate frame is indicated by a '0' as the leading superscript. Line nodes are indicated with two entries in the trailing subscript; the first representing the line in its entirety, and the second representing the node within that line.

3.1. Fluid flow characteristics

For any useful results to be obtained, it is important to accurately describe the way water flows through the space occupied by a tidal turbine system. The simplest case is one of uniform fluid velocity throughout the entire domain. Unfortunately, this condition is not observed at tidal energy sites since ambient turbulence and spatial variation of the mean flow velocity is characteristic of the energetic flows suitable for tidal energy extraction [16]. Although the bulk fluid flow characteristics for a given site are approximated by tidal harmonic modelling, there is no way to determine the local temporal flow on length-scales relevant to tidal energy devices, which is subject to ambient turbulence, surface wave effects, and large scale eddies. Due to the stochastic nature of these effects, they are best modelled via statistical methods, and therefore it is necessary to develop a method to generate a representative time-domain fluid velocity vector field based on the bulk flow and the turbulence intensity characteristics at a specific site. Turbulence intensity is defined as the ratio of the local velocity fluctuations, quantified as the standard deviation of flow speed, to the mean flow. This value is typically site-specific, though values obtained from limited field data at proposed tidal turbine deployment sites are in the vicinity of 10% [17].

Accounting for turbulence in the fluid velocity is important for compliant-moored systems as it can cause unwanted oscillatory motion of a device. Turbulent fluctuation-induced oscillations near a resonant mode can cause significant motion of the turbine or mooring elements. An understanding of

the dynamic behavior of a device operating in turbulent flow conditions would assist turbine developers in the design of mooring configurations that are not adversely affected by turbulence.

Though it is necessary to implement a suitable model of fluid turbulence to obtain useful results for mooring design applications, it must first be shown that results obtained for systems in the absence of turbulence reasonably match experimental observations. Since the focus of this paper is on the development of the mathematical description of the system and preliminary validation, the fluid flow at this stage of development is defined simply as an analytical function of time and space. Each component of velocity along the inertial coordinate directions is defined separately.

$${}^0\vec{V}_{Fluid} = \begin{bmatrix} V_x(x, y, z, t) \\ V_y(x, y, z, t) \\ V_z(x, y, z, t) \end{bmatrix}$$

Defining fluid velocity in this way is suitable for flows whose velocity profiles can be easily described analytically, however, this is likely not the case for turbulent flows. Therefore, later development of the simulation will allow the fluid velocity to be defined as a vector field, wherein the three components of velocity will be defined as functions of time at each point within a three-dimensional grid. In this way, the velocity at any point in space and time can be reasonably approximated as a linear interpolation between adjacent grid locations. This full-field method is employed by the turbulence simulator TurbSim (wind.nrel.gov/designcodes/preprocessors/turbsim), which provides a numerical simulation of flow containing coherent turbulent structures [18].

3.2. Device Configuration

A basic system that can be modeled using the described techniques is that shown in Figure 5, wherein a single buoyant tidal turbine is submerged in a tidal flow and tethered to the sea floor by two flexible

mooring lines. A ducted tidal turbine is shown simply for illustrative purposes; the code allows for modeling of a wide range of turbine types through proper parameterization of the turbines.

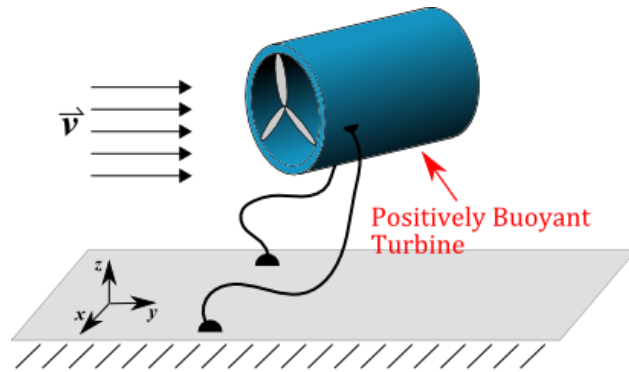


Figure 5: Simple Single Turbine System

Multiple mooring lines can be connected by inserting a free node, which creates a junction of zero mass allowing for sophisticated mooring cable configurations to be evaluated. A simple example of a system utilizing a free node is shown in Figure 6.

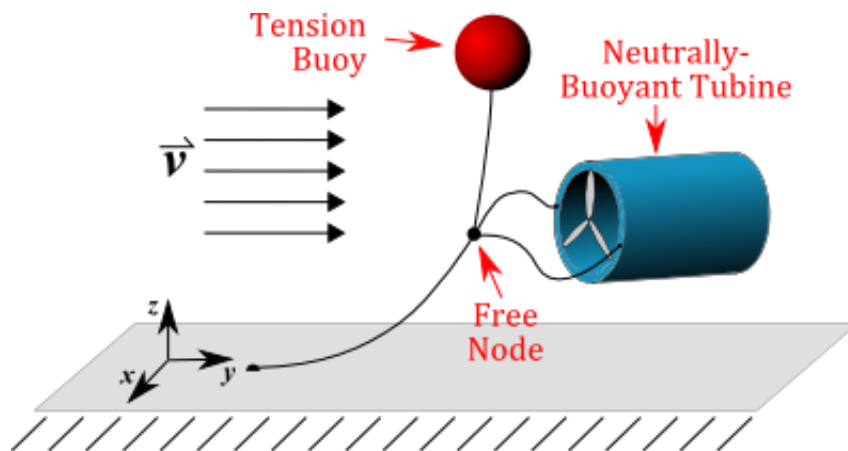


Figure 6: Single point tensioned tidal turbine featuring one free node

More complex systems are capable of possessing multiple rigid bodies connected via mooring lines to the sea floor or to other bodies. Rigid bodies can also be connected by links in such a way that one body is constrained to a fixed position within another body's fixed coordinate frame, as shown in Figure 7.

One turbine is arbitrarily selected as the ‘free body’ and the other is defined as being constrained to a specified location within the body-fixed frame belonging to the free body.

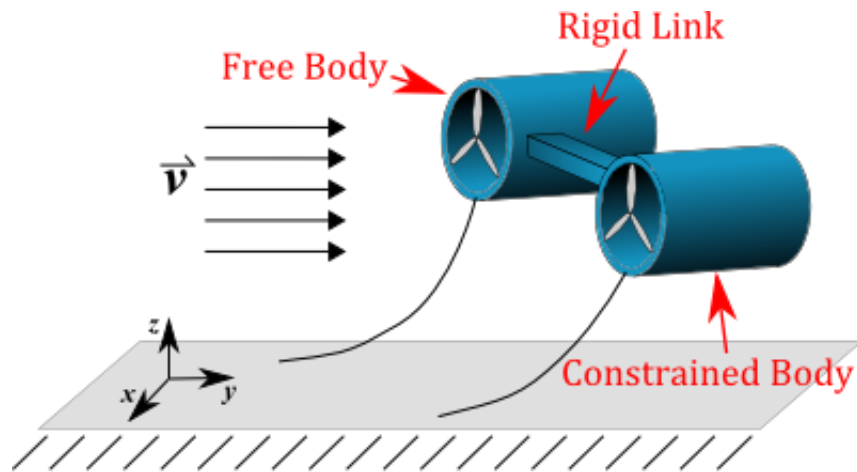


Figure 7: Tidal turbine system featuring one free turbine and one constrained turbine

Of interest are the motion of the turbines within the tidal flow and the tension experienced by the lines. This information will allow turbine developers to verify that a particular design will behave as desired with respect to how the turbine is oriented during a changing fluid flow. Furthermore, it will reveal useful information about the structural loading experienced by a device throughout its intended range of operational conditions, allowing developers to make more informed decisions regarding materials and structural characteristics of a proposed design.

To facilitate the calculations required to model the continuously flexible mooring lines, a discretization method is adopted. Each line is divided into a number of discrete segments specified by the user. The greater the number of segments, the more closely the model will resemble a continuous mooring line until the point where the number of segments is so great that the length of each segment has an order of magnitude comparable to the computer’s floating point precision and rounding errors begin to dominate. Furthermore, each additional line segment introduces three additional degrees of freedom to the system (one in each coordinate direction), which increases the computation time required to

solve the system. An appropriate balance must be found between a sufficiently realistic model and one that can be solved in a reasonable amount of time.

3.2.1. Rigid bodies

At this stage of development, the hydrokinetic turbines and any additional devices or structures are modeled as simple rigid bodies. This greatly simplifies the calculation of the fluid forces acting on the system. Once the program dependably solves systems using this approach, refinements will be made to more accurately calculate the fluid forces on complex geometries, as well as account for other effects such as turbulence and energy extraction by the turbines, however for the initial development of the code rigid body mechanics are sufficient. These bodies have properties such as mass and buoyancy, moments of inertia about the body-fixed axes, drag coefficients corresponding to flow in the directions of the body-fixed axes, and characteristic area used in the drag force calculation along each body-fixed axis. It is assumed that the component of fluid velocity parallel to a body-fixed axis imparts a drag force which is also parallel to that axis, i.e. no lift. The lift experienced by symmetric bodies at non-zero angles of attack is approximated by splitting the relative fluid velocity into its components along the body-fixed axes and using corresponding drag coefficients and characteristic areas for flow along each coordinate direction. This approach is suitable for blunt body geometries, assuming the flow possesses a sufficiently high Reynolds number.

3.2.2. Mooring lines

The possibilities for mooring line configurations and characteristics are endless. A simple approach is to use a single line anchoring the tidal turbine to the seafloor. This method allows the turbine to automatically transition between incoming and outgoing tidal current, but also requires a great deal of space to any adjacent objects to provide enough room for the turbine to move about. Another approach is to employ several mooring lines to keep the turbine confined to a smaller spatial region,

which has its own set of advantages and limitations. Furthermore, arrays of tidal turbines can either be individually anchored or lines can be attached between several turbines. The most suitable approach depends on the specific site characteristics.

In addition to how the lines are configured, the materials used for the lines are also important. Choices for line materials can range from steel cables or chains to heavy nylon cord or rope. Properties input for each mooring line include the user-defined number of segments into which to divide the line, coordinates for the line starting and ending points, the spring constant for a line of unit length from which the total line spring constant is calculated, mass per unit length, diameter, and drag coefficients for flow parallel and perpendicular to the axis of the line segment.

3.3. Kinematics

Figure 8 shows the free-body diagram of a rigid body within a simply configured system and Figure 9 shows the forces acting on an individual line node. The rigid body is subjected to forces due to gravity, buoyancy, mooring-line tension, and fluid drag.

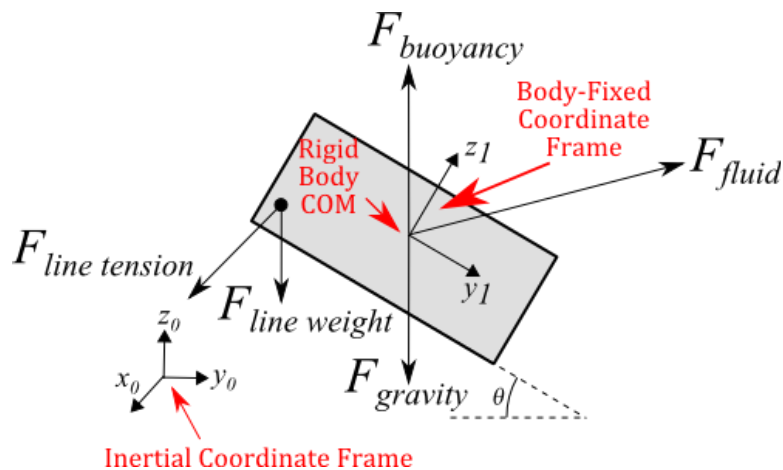


Figure 8: Rigid Body Kinematic System

An elastic line connecting the rigid body to an inertial coordinate frame is divided into discrete straight segments, and each segment is subjected to forces applied at its end nodes. Figure 9 shows two line segments and the forces acting on the node shared by each segment.

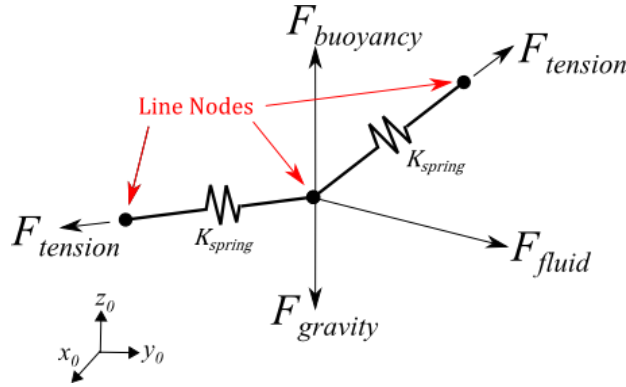


Figure 9: Line Segment Kinematic System

A complete model will result in a system of differential equations of motion in the familiar form of Equation (1), where M is a mass matrix, B is a damping coefficient matrix (if external damping is applied), K is a stiffness matrix, and F is an array of forces acting on the corresponding displacement variable consisting of the contributions from drag, gravity, buoyancy, and any applied forces. The inequality array $g(x) \geq 0$ contains all constraints to which the displacement variables are subject. These constraints account for the effects of line slackness (since the instantaneous length of a line segment cannot be less than the line segment's natural length) as well as the effect of seafloor impenetrability, both of which are discussed in a later section of this paper.

$$M\ddot{x} + B\dot{x} + Kx = F(x, \dot{x}, \ddot{x}, t) \quad (1)$$

The equations of motion of the system are derived through implementation of Lagrange's Equation of Motion, which is discussed in detail in Section 3.4.

3.3.1. Rigid Body Euler Angles

There has been much more work done to describe the motion of wave energy converters than there has for compliant-moored tidal turbines. Unfortunately, most of these models only consider small rotations of the device and therefore apply the small angle theorem to simplify the model (e.g. [19], [20]). Here, we wish to solve systems where large rotations are expected and therefore the small angle theorem does not apply. It follows that each rigid body in the system carries with it a total of six independent variables (degrees of freedom) corresponding to translations in three-dimensional space as well as rotations about its body-fixed axes. This presents a challenge to appropriately account for angular displacements and velocities, since many calculations require transformations of coordinates and vectors between the body-fixed frames and the inertial frame. To this end, angular displacements and velocities of the rigid bodies are expressed in terms of α - β - γ Euler Angles as shown in Figure 10. In this manner, any point or vector in the body-fixed frame can be expressed in the global frame with a simple multiplication by a transformation matrix.

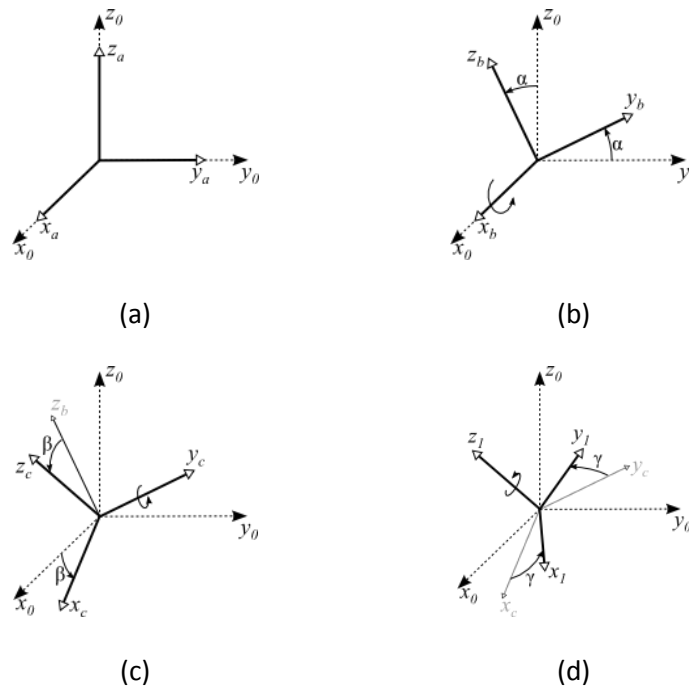


Figure 10: Euler Angle Coordinate Transformation

To derive the transformation matrix, we begin with the coordinate frame 'a', coincident to the inertial frame as shown in Figure 10(a). Frame 'a' is then rotated about its x_a -axis by an angle α to frame 'b', as shown in Figure 10(b). Any vector represented in terms of frame 'b' can be expressed in the inertial coordinate frame using the transformation

$${}^0\vec{r} = {}^a\vec{r} = \begin{bmatrix} 1 & 0 & 0 \\ 0 & c_\alpha & -s_\alpha \\ 0 & s_\alpha & c_\alpha \end{bmatrix} {}^b\vec{r}.$$

Note that the superscript preceding the vector identifies the coordinate frame in which the vector is expressed, and the shorthand notation c_α and s_α is used to represent $\cos(\alpha)$ and $\sin(\alpha)$, respectively. Continuing along, frame 'b' is rotated by an angle β about its y_b -axis to frame 'c', as shown in Figure 10(c). A vector in frame 'c' can be expressed in frame 'b' as

$${}^b\vec{r} = \begin{bmatrix} c_\beta & 0 & s_\beta \\ 0 & 1 & 0 \\ -s_\beta & 0 & c_\beta \end{bmatrix} {}^c\vec{r}.$$

Finally, frame 'c' is rotated about its z_c -axis by the angle γ to obtain the body-fixed frame 'i'. A vector in the body-fixed frame can be expressed in frame 'c' as

$${}^c\vec{r} = \begin{bmatrix} c_\gamma & -s_\gamma & 0 \\ s_\gamma & c_\gamma & 0 \\ 0 & 0 & 1 \end{bmatrix} {}^i\vec{r}.$$

Using these three successive transformations, a vector expressed in the body-fixed frame can be obtained with respect to the inertial frame by

$${}^0\vec{r} = \bar{\bar{A}}_i {}^i\vec{r} \quad (2)$$

where $\bar{\bar{A}}_i$ is the direction cosine matrix for body-fixed frame 'i' obtained by successive matrix multiplication of the three intermediate matrices:

$$\begin{aligned}\bar{\bar{A}}_i &= \begin{bmatrix} 1 & 0 & 0 \\ 0 & c_\alpha & -s_\alpha \\ 0 & s_\alpha & c_\alpha \end{bmatrix} \begin{bmatrix} c_\beta & 0 & s_\beta \\ 0 & 1 & 0 \\ -s_\beta & 0 & c_\beta \end{bmatrix} \begin{bmatrix} c_\gamma & -s_\gamma & 0 \\ s_\gamma & c_\gamma & 0 \\ 0 & 0 & 1 \end{bmatrix} \\ &= \begin{bmatrix} c_\beta c_\gamma & -c_\beta s_\gamma & s_\beta \\ s_\alpha s_\beta c_\gamma + c_\alpha s_\gamma & -s_\alpha s_\beta s_\gamma + c_\alpha c_\gamma & -s_\alpha c_\beta \\ -c_\alpha s_\beta c_\gamma + s_\alpha s_\gamma & c_\alpha s_\beta s_\gamma + s_\alpha c_\gamma & c_\alpha c_\beta \end{bmatrix}_i.\end{aligned}\quad (3)$$

Additionally, a point in a body-fixed frame whose origin is not coincident with that of the inertial frame can be found by

$${}^0\vec{P}_i = {}^0\vec{P}_j + \bar{\bar{A}}_j {}^j\vec{P}_i \quad (4)$$

where ${}^0\vec{P}_j$ is the location of the origin of the body-fixed frame 'j' with respect to the inertial frame '0' and ${}^j\vec{P}_i$ is the location of point 'i' with respect to the body-fixed frame.

It is also necessary to find the velocity of a point on a translating and rotating rigid body expressed as a vector in global coordinates in terms of the velocity of the origin of the body and the time derivative of its α - β - γ Euler angles. The angular velocity of the body-fixed frame can be written in terms of its Euler Angles as

$${}^i\vec{\omega}_i = \dot{\alpha}\hat{i}_a + \dot{\beta}\hat{j}_b + \dot{\gamma}\hat{k}_c \quad (5)$$

where \hat{i}_a , \hat{j}_b , and \hat{k}_c are the unit vectors along the x_a , y_b , and z_c axes, respectively, as shown in Figure 10. Noting that the x_a axis is parallel to the inertial x_0 -axis, it follows that the unit vector \hat{i}_a is parallel to the global \hat{i}_0 unit vector, therefore $\hat{i}_a = \hat{i}_0$. The vector \hat{i}_0 can be obtained in terms of the body-fixed frame unit vectors \hat{i}_i , \hat{j}_i , and \hat{k}_i using the transformation matrix derived above:

$$\begin{bmatrix} \hat{i}_0 \\ \hat{j}_0 \\ \hat{k}_0 \end{bmatrix} = \begin{bmatrix} \hat{i}_a \\ \hat{j}_a \\ \hat{k}_a \end{bmatrix} = \bar{\bar{A}} \begin{bmatrix} \hat{i}_i \\ \hat{j}_i \\ \hat{k}_i \end{bmatrix} = \begin{bmatrix} c_\beta c_\gamma & -c_\beta s_\gamma & s_\beta \\ s_\alpha s_\beta c_\gamma + c_\alpha s_\gamma & -s_\alpha s_\beta s_\gamma + c_\alpha c_\gamma & -s_\alpha c_\beta \\ -c_\alpha s_\beta c_\gamma + s_\alpha s_\gamma & c_\alpha s_\beta s_\gamma + s_\alpha c_\gamma & c_\alpha c_\beta \end{bmatrix} \begin{bmatrix} \hat{i}_i \\ \hat{j}_i \\ \hat{k}_i \end{bmatrix}$$

$$\Rightarrow \hat{i}_a = c_\beta c_\gamma \hat{i}_i - c_\beta s_\gamma \hat{j}_i + s_\beta \hat{k}_i.$$

Similarly, the unit vector \hat{j}_b can be obtained in terms of the body-fixed frame unit vectors using the second two transformation matrices in the series:

$$\begin{bmatrix} \hat{i}_b \\ \hat{j}_b \\ \hat{k}_b \end{bmatrix} = \begin{bmatrix} c_\beta & 0 & s_\beta \\ 0 & 1 & 0 \\ -s_\beta & 0 & c_\beta \end{bmatrix} \begin{bmatrix} c_\gamma & -s_\gamma & 0 \\ s_\gamma & c_\gamma & 0 \\ 0 & 0 & 1 \end{bmatrix} \begin{bmatrix} \hat{i}_i \\ \hat{j}_i \\ \hat{k}_i \end{bmatrix}$$

$$\Rightarrow \hat{j}_b = s_\gamma \hat{i}_i + c_\gamma \hat{j}_i.$$

And finally, the unit vector \hat{k}_c is obtained from the last transformation matrix in the series or by observation that \hat{k}_c is parallel to \hat{k}_i :

$$\hat{k}_c = \hat{k}_i.$$

The angular velocity of the body-fixed frame can now be expressed in terms of Euler Angles as:

$${}^i\vec{\omega}_i = \dot{\alpha}(c_\beta c_\gamma \hat{i}_i - c_\beta s_\gamma \hat{j}_i + s_\beta \hat{k}_i) + \dot{\beta}(s_\gamma \hat{i}_i + c_\gamma \hat{j}_i) + \dot{\gamma} \hat{k}_i$$

$${}^i\vec{\omega}_i = \begin{bmatrix} c_\beta c_\gamma & s_\gamma & 0 \\ -c_\beta s_\gamma & c_\gamma & 0 \\ s_\beta & 0 & 1 \end{bmatrix} \begin{bmatrix} \dot{\alpha} \\ \dot{\beta} \\ \dot{\gamma} \end{bmatrix}. \quad (6)$$

With the angular velocity of the body-fixed frame known, the velocity of any fixed point in that frame with respect to the inertial coordinate system can be calculated as

$${}^0\vec{v} = {}^0\vec{v}_i + \bar{\bar{A}}_i ({}^i\vec{\omega} \times {}^i\vec{P}) \quad (7)$$

where ${}^0\vec{v}_i$ is the velocity of the origin of the body-fixed frame 'i' with respect to the inertial frame and ${}^i\vec{P}$ is the location of the body-fixed point of interest with respect to the body-fixed frame.

Implementation of α - β - γ Euler Angles to keep track of rigid body rotation and angular velocity adds additional degrees of freedom and significantly increases the complexity of the system when compared to models that apply the small angle theorem, but it allows for large rotations and angular velocities to

be accounted for by the model. This opens up a wide range of problems which can be analyzed using these methods.

3.3.2. Line discretization

The computation for the effects of the mooring lines are carried out using a discretization method approach. Each line in the system is divided into a finite number of segments defined by the user in the system configuration file and all line parameters are lumped into equally spaced nodes. Since both end points on each line are constrained to a fixed point in either the inertial frame or a body-fixed frame, they do not add to the total number of degrees of freedom of the system. The inner nodes, however, add three degrees of freedom each (for x , y , and z displacements), and there are one fewer inner nodes than segments of each line. For example, a line divided into thirty-two segments will add $(32 - 1)(3) = 93$ degrees of freedom.

All contributions to the dynamics of the system resulting from forces on the mooring lines are lumped to the line nodes. The nodes are modeled as point masses connected by linear springs. The whole mass of the line is distributed equally amongst the nodes. Drag forces are calculated for each individual line segment, modeled as a thin cylinder with drag acting in a direction tangential and normal to the line segment. The instantaneous force which is calculated to be acting on a line segment is then distributed evenly to the two nodes on either end of the line segment.

3.4. Lagrange's Equation of Motion

Using a Lagrangian reference frame, Lagrange's Equation of Motion, given as equation (8) below, is implemented to generate the complete system of differential equations which describes the system. The number of equations in the system is equal to the number of degrees of freedom determined by the number of rigid bodies, free nodes, and mooring line segments.

$$\frac{d}{dt} \frac{\partial T}{\partial \dot{q}_i} - \frac{\partial T}{\partial q_i} + \frac{\partial V}{\partial q_i} + \frac{\partial D}{\partial \dot{q}_i} = e_i \quad (8)$$

T , V , and D are scalar symbolic expressions for the total kinetic energy, the total potential energy, and the rate of energy dissipated due to linear damping terms, respectively, q and \dot{q} are the symbolic arrays of displacement and velocity variables, respectively, and e is the array containing symbolic expressions for the forces acting on each independent displacement variable. The symbolic expressions for T , V , D , and each entry in e are non-linear functions of q , \dot{q} , and t .

The result of Lagrange's equation is a system of differential equations, one corresponding to each degree of freedom of the system, and all of which are functions only of q , \dot{q} , \ddot{q} , and time t . The most complicated term to deal with numerically in this equation is the first since it requires a total differentiation with respect to time after a partial derivative is taken with respect to velocity. A given system could potentially have thousands of degrees of freedom, so it is clear that computerized methods for deriving the system of equations that results from implementation of Lagrange's equation are necessary. The methods for obtaining the symbolic expressions for the three energy terms and the forces acting on the independent variables are described in the following sections.

3.5. Kinetic Energy

To derive the equations of motion using Lagrange's equation, an expression for the total kinetic energy as a function of the independent variables is needed. The total kinetic energy is simply the sum of the kinetic energies of all individual mass-possessing elements of the system. The general equation for the translational kinetic energy of a body is

$$T_{trans} = \frac{1}{2}m \|\mathbf{v}\|^2 = \frac{1}{2}m(v_x^2 + v_y^2 + v_z^2) \quad (9)$$

where m is the mass of the object, v is its velocity in the inertial frame, and v_x , v_y , and v_z are the components of velocity in the x, y, and z directions. Rotational kinetic energy is calculated as

$$T_{rotate} = \frac{1}{2} I_i \| {}^i \vec{\omega} \|^2 = \frac{1}{2} (I_x \omega_x^2 + I_y \omega_y^2 + I_z \omega_z^2) \quad (10)$$

where I_i is the moment of inertia about the body-fixed i -axis and ω_i is the angular velocity about that axis. Because the mooring lines are discretized into a finite number of segments and their mass is lumped to point-nodes, only the rigid bodies in the system experience rotational kinetic energy.

The rotational kinetic energy is obtained by first finding the angular velocity of the body about its own body-fixed coordinate frame, i.e. ${}^i \vec{\omega}_i = {}^i [\omega_{x,i} \quad \omega_{y,i} \quad \omega_{z,i}]$. Since the symbolic velocity vector expresses the rigid body angular velocities in terms of time derivatives of Euler angle rotations, a transformation is needed to find the appropriate expressions for angular velocity about the body-fixed coordinate frame axes. This is accomplished using the transformation matrix defined in Equation (6), which yields the three axial components of the angular velocity of a rigid body as functions of the displacement variables α , β , and γ and the velocity variables $\dot{\alpha}$, $\dot{\beta}$, and $\dot{\gamma}$ belonging to the body. An expression for the kinetic energy of a body is then found from these angular velocity expressions and the translational velocities of the body to be

$$T_{Body,i} = \frac{1}{2} (m_i (\dot{x}_i^2 + \dot{y}_i^2 + \dot{z}_i^2) + I_{x,i} \omega_{x,i}^2 + I_{y,i} \omega_{y,i}^2 + I_{z,i} \omega_{z,i}^2). \quad (11)$$

Expressing the kinetic energy of a constrained body requires additional calculation due to the fact that the displacement of such a body is defined by the displacement of the free body to which it is fixed. The kinetic energy of a constrained body is therefore expressed as a symbolic function of its parent body's displacement variables. The translational velocity of the center of mass of a constrained body is found from the translational and rotational velocity of the coordinate frame to which it is fixed, i.e. that of its parent body, as

$${}_{CB}^0 \vec{V}_i = {}_B^0 \vec{V}_j + \bar{A}_j(\alpha_j, \beta_j, \gamma_j) ({}_B^j \vec{\omega}_j \times {}_{CB}^j \vec{r}_i) \quad (12)$$

where the index j refers to the body to which the constrained body is fixed and ${}_{CB}^j \vec{r}_i$ is the vector from the origin of frame j to that of the constrained body i . It is necessary to multiply the cross product

${}^j_B\vec{\omega}_j \times {}^j_{CB}\vec{r}_i$ by the Euler Angle transformation matrix \bar{A}_j due to the fact that the coordinate frame j is able to rotate with respect to the inertial frame. The rotational velocity of a constrained body is equal to that of its parent coordinate frame multiplied by the direction cosine matrix relating vectors in the constrained body-fixed frame to the free body-fixed frame. This direction cosine matrix is constant throughout the simulation since a constrained body is not free to rotate relative to its parent body. Furthermore, this matrix evaluates to the 3x3 identity matrix if the constrained body-fixed frame axes are parallel to the corresponding axes in the parent body-fixed frame. Therefore the kinetic energy of a constrained body is

$$T_{ConBody,i} = \frac{1}{2} \left(m_i ({}^0_{CB}\vec{V}_i \cdot {}^0_{CB}\vec{V}_i) + I_{x,i} ({}^i_{CB}\omega_{x,i})^2 + I_{y,i} ({}^i_{CB}\omega_{y,i})^2 + I_{z,i} ({}^i_{CB}\omega_{z,i})^2 \right) \quad (13)$$

$${}^0_{CB}\vec{V}_i = f(\dot{x}_j, \dot{y}_j, \dot{z}_j, \dot{\alpha}_j, \dot{\beta}_j, \dot{\gamma}_j)$$

$${}^i_{CB}\vec{\omega}_i = {}^i_B\vec{\omega}_j = \bar{A}_i^{-1} {}^j_B\vec{\omega}_j = f(\dot{\alpha}_j, \dot{\beta}_j, \dot{\gamma}_j)$$

It is also necessary to derive a symbolic expression for the kinetic energy of the mooring lines. Using the lumped-parameter approach for the mooring lines, the kinetic energy for each line is found as the sum of the individual kinetic energies of each lumped mass. If an end of a mooring line is fixed to a rigid body, then the velocity of an end-node is found in the same manner as the velocity of a constrained body. Lumped-parameter line nodes are considered as point-masses, and therefore any rotation experienced by a line node does not contribute to the angular kinetic energy of the system. The kinetic energy of a line end-node is

$$T_{Line,i,End} = \frac{1}{2} \frac{m_{segment,i}}{2} ({}^0_{LN}\vec{V}_{i,End} \cdot {}^0_{LN}\vec{V}_{i,End}) \quad (14)$$

Taking one-half of the line segment mass is consistent with the lumped-parameter approach as only half the mass of a line segment is lumped to the end-nodes. The kinetic energy of an end-node of a line

terminating at a free node is easily calculated owing to the fact that the displacement of a free node is directly accounted for in the q -displacement array.

$$T_{Line,i,End} = \frac{1}{2} \frac{m_{segment,i}}{2} (\dot{x}_j^2 + \dot{y}_j^2 + \dot{z}_j^2) \quad (15)$$

where the index j refers to the free node to which the line terminus is attached. Finally, the kinetic energy of a line terminus fixed to the inertial frame is zero.

The kinetic energy of the remaining interior line nodes is calculated in a manner similar to that of a line terminus at a free node since the displacement of these nodes are also independent variables accounted for in the q -displacement variable array.

$$T_{Line,i,Node,j} = \frac{1}{2} m_{segment,i} (\dot{x}_{i,j}^2 + \dot{y}_{i,j}^2 + \dot{z}_{i,j}^2) \quad (16)$$

Here, the line segment mass is not factored by one-half since for all interior line nodes there is a lumped-mass contribution from two adjacent line segments of equal mass.

The total kinetic energy of the system is found as the sum of all individual kinetic energy components.

$$\begin{aligned} T_{Total} = & \left[\sum_{i=1}^{NumBody} T_{Body,i} \right] + \left[\sum_{i=1}^{NumConBody} T_{ConBody,i} \right] \\ & + \left[\sum_{i=1}^{NumLine} (T_{Line,i,Start} + T_{Line,i,End}) \right] \\ & + \left[\sum_{i=1}^{NumLine} \sum_{j=1}^{NumNode} T_{Line,i,Node,j} \right] = f(\bar{q}, \dot{\bar{q}}) \end{aligned} \quad (17)$$

where \bar{q} is the array of independent displacement variables and $\dot{\bar{q}}$ is its time derivative, i.e. the array of independent velocity variables.

3.6. Potential Energy

A symbolic expression for the total potential energy of the system as a function of the independent displacement variables is also needed to implement Lagrange's equation of motion. Potential energy is stored in the elastic mooring lines, modelled as an assemblage of discrete spring segments. The amount of potential energy stored in each segment is

$$V = \frac{1}{2}k(\ell - \ell_0)^2 \quad (18)$$

where k is the segment spring constant, ℓ is the instantaneous segment length, and ℓ_0 is the unstretched segment length. The calculation for the instantaneous length of the line segments at either end of a mooring line is dependent on the feature to which the end is attached. For a mooring line end fixed to a rigid body, the instantaneous position of the attachment point on the rigid body first must be found.

$${}_{LN}^0\vec{P}_{i,End} = (x_j + y_j + z_j) + \bar{A}_j(\alpha_j, \beta_j, \gamma_j)({}_{LN}^j\vec{r}_{i,End}) \quad (19)$$

where the index j refers to the body to which the line terminus is attached and ${}_{LN}^j\vec{r}_{i,end}$ is the fixed location of the mooring line attachment point in the body-fixed coordinate frame j . Since the position of a free node is accounted for in the q -displacement array, the position of a mooring line end terminating at a free node is

$${}_{LN}^0\vec{P}_{i,End} = ({}_{FN}^0x_j + {}_{FN}^0y_j + {}_{FN}^0z_j) \quad (20)$$

where the index j refers to the free node to which the line terminus is attached. The position of a mooring line end fixed to the inertial frame is

$${}_{LN}^0\vec{P}_{i,End} = ({}_{LN}^0X_{i,End} + {}_{LN}^0Y_{i,End} + {}_{LN}^0Z_{i,End}) \quad (21)$$

The uppercase displacement variables indicate that these quantities are constant with respect to the inertial frame. The position of the line node adjacent to the attachment point is accounted for as an

independent variable in the q -displacement variable array, therefore the instantaneous length of the corresponding line segment is

$$\begin{aligned} \ell &= \left\| {}_{LN}^0\vec{P}_{i,End} - {}_{LN}^0\vec{P}_{i,End-1} \right\| \\ &= \left\| {}_{LN}^0\vec{P}_{i,End} - \begin{bmatrix} {}_{LN}^0x_{i,End-1} & {}_{LN}^0y_{i,End-1} & {}_{LN}^0z_{i,End-1} \end{bmatrix}^T \right\| \end{aligned} \quad (22)$$

The instantaneous length of an interior line segment is simpler to calculate since both of the relevant line node positions are directly accounted for in the q -displacement variable array.

$$\begin{aligned} \ell &= \left\| {}_{LN}^0\vec{P}_{i,j} - {}_{LN}^0\vec{P}_{i,j+1} \right\| \\ &= \sqrt{({}_{LN}^0x_{i,j} - {}_{LN}^0x_{i,j+1})^2 + ({}_{LN}^0y_{i,j} - {}_{LN}^0y_{i,j+1})^2 + ({}_{LN}^0z_{i,j} - {}_{LN}^0z_{i,j+1})^2} \end{aligned} \quad (23)$$

Plugging the above symbolic expressions for the instantaneous length of a line segment into (18) yields the potential energy stored in the corresponding line segment. The total potential energy is found by summing the individual potential energies of each line segment in the system. It should be noted that the gravitational potential energy of elements in the system is not included in the expression for the total potential energy due to the fact that weight and buoyancy are modeled as forces acting on the system rather than contributing to the potential energy of the system.

3.7. Rate of Energy Dissipation

It may happen that users of this program will want to add linear damping terms to a system. These terms may reflect the contribution from mechanical dampers included in the system, or they may be used to account for expected fluid loading that is not well-modeled by drag or other known phenomena. In the latter case, the damping term can be treated as a tuning parameter.

The rate at which energy is removed from the system by damping is related to the speed of the damped feature and the damping coefficient, B .

$$D = \frac{1}{2}B\|{}^0\bar{V}\|^2 \quad (24)$$

The expression for the total linear damping, if utilized, is found as the sum of all individual damping terms. The symbolic expression for damping applied to an individual feature is easily found from the velocity variables that correspond to that feature. If the damped feature is a constrained body or a mooring line end-node fixed to a rigid body, then its velocity is found using the methods described in Section 3.3. For the purposes of this paper, linear damping is modeled as a single value representing damping opposing motion in all three coordinate directions, as well as a single value for rotational damping about all three coordinate axes for a rigid body.

If through implementation of this simulation it is found that more specific linear damping terms are needed, such as different damping coefficients for motion in various directions, this functionality can be expanded to allow for greater detail.

3.8. Force Contributors

The forces acting on each element of the system are assembled into an array e , which is used to derive the equations of motion for each independent variable by implementation of Lagrange's equation. Each entry in e corresponds to a force or moment affecting a particular independent displacement variable and must be expressed with respect to the inertial frame for consistency with the expressions for kinetic, potential, and damping energy. There are six entries in e corresponding to forces acting on the x , y , and z displacements and the α , β , and γ Euler angle rotations of each unconstrained rigid body in the system. The forces acting on a constrained body are translated to forces and couple moments acting on the parent body. Line nodes and free nodes have only three entries in e each, corresponding to forces acting on x , y , and z displacements.

3.8.1. Gravity

The gravitational force experienced by a rigid body acts through the center of mass. Since the COM also defines the origin of the body-fixed frame, accounting for the force due to gravity is simple for unconstrained rigid bodies.

$${}^0_B(\vec{F}_{grav})_i = -m_i g \hat{k}$$

Therefore the six entries in the force array corresponding to the gravitational force on the unconstrained body i are

$${}^0_B[e_x \ e_y \ e_z \ e_\alpha \ e_\beta \ e_\gamma]_i = [0 \ 0 \ -m_i g \ 0 \ 0 \ 0]$$

The gravitational force acting on a constrained body requires more calculation due to the fact that the displacement of a constrained body is not included in the array of independent displacement variables. As a result, the gravitational force acting on a constrained body is translated to the parent body, which will experience the force as well as a resulting moment couple. The force experienced by the parent body (j) is equal to that of the constrained body (i), expressed in the global frame.

$${}^0_B(\vec{F}_{grav})_j = {}^0_{CB}(\vec{F}_{grav})_i = -m_i g \hat{k}$$

To find the moment experienced by the parent body due to the force of gravity applied to the constrained body, the gravitational force is first transformed to a vector expressed in the body-fixed frame j using the inverse of the Euler Angle transformation matrix.

$${}^j_{CB}(\vec{F}_{grav})_i = \bar{A}_j^{-1} {}^0_{CB}(\vec{F}_{grav})_i \quad (25)$$

The resulting moment experienced by the parent body is calculated as the cross product of the vector from the origin of the parent body-fixed frame to the COM of the constrained body (${}^j_{CB}\bar{P}_i$) and the force

of gravity expressed in the body-fixed frame. This moment, expressed in the body fixed frame j , is then transformed to the inertial frame with another operation with the Euler Angle transformation matrix.

$${}^0_B(\bar{M}_{grav})_j = \bar{A}_j^j({}^j_B\bar{M}_{grav})_j = \bar{A}_j \left({}_{CB}^j\bar{P}_i \times {}_{CB}^j(\bar{F}_{grav})_i \right) \quad (26)$$

Therefore the six entries in the force array corresponding to the gravitational force on the constrained body i are expressed as forces on the parent body j as

$${}^0_B[e_x \ e_y \ e_z \ e_\alpha \ e_\beta \ e_\gamma]_j = \left[0 \ 0 \ -m_i g \quad {}^0_B(M_{grav})_{j,\alpha} \quad {}^0_B(M_{grav})_{j,\beta} \quad {}^0_B(M_{grav})_{j,\gamma} \right]$$

Using the lumped-parameter approach, the gravitational force experienced by a line segment of mass m_{seg} is evenly distributed to the nodes enclosing that segment. Special consideration must be taken when one of those nodes is a line terminus. If such a node is fixed to the inertial frame, then the system is unaffected by the gravitational force to which that node is subjected. If the line terminates at a free node, the force of gravity is applied to the z -displacement variable corresponding to that node. If, however, this node is fixed to a rigid body, free or constrained, the gravitational force experienced by the node translates to a force and moment couple applied to the free body. Though this is a similar case to that of the force of gravity on a constrained body being translated to the parent body, it is handled in a different manner. First, the velocity of node i is found with respect to the body-fixed frame as the cross product of the angular velocity of rigid body j and the position of the line node within that frame. The velocity of the node with respect to the inertial frame is then found using the Euler Angle transformation of the velocity in the body-fixed frame and adding the result to the translational velocity of the rigid body.

$${}_{LN,End}^0\bar{V}_i = {}^0_B\bar{V}_j + \bar{A}_j({}^0_B\bar{\omega}_j \times {}_{LN,End}^j\bar{P}_i) \quad (27)$$

If the body to which the node is attached is a free body, the index j in the above equation refers to that body. If, however, the line terminus node is attached to a constrained body, then j refers to that body's

parent. Next, the rate at which work is performed (i.e. power) on the free body is found as the dot product of the gravitational force vector and the node velocity vector expressed in the inertial frame. Finally, the moment couple is calculated component-wise as the derivative of power with respect to the corresponding Euler angular velocity components.

$${}^0_B(\bar{M}_{grav})_j = \left[\frac{\partial}{\partial \dot{\alpha}} \quad \frac{\partial}{\partial \dot{\beta}} \quad \frac{\partial}{\partial \dot{\gamma}} \right]^T \left(\begin{bmatrix} 0 & 0 & -\frac{1}{2}g(m_{seg})_i \end{bmatrix} \cdot {}^0_{LN}\vec{V}_{i,End} \right) \quad (28)$$

Therefore, the six entries in the force array corresponding to the gravitational force acting on the terminus node of line i , which is attached to a rigid body, are expressed as forces on the unconstrained rigid body j as

$${}^0_B[e_x \quad e_y \quad e_z \quad e_\alpha \quad e_\beta \quad e_\gamma]_j = \begin{bmatrix} 0 & 0 & -\frac{1}{2}g(m_{seg})_i & {}^0_B(M_{grav})_{j,\alpha} & {}^0_B(M_{grav})_{j,\beta} & {}^0_B(M_{grav})_{j,\gamma} \end{bmatrix}$$

The gravitational force acting on the interior nodes of a mooring line and on free nodes are easily accounted for in the force array e since the z -displacements of these nodes are included as independent variables.

3.8.2. Buoyancy

The force of buoyancy acts through the geometric center of a completely submerged body with a magnitude equal to the weight of seawater displaced by the body. At this stage of development, it is assumed that the body has either a uniform density or symmetry such that the center of mass and the geometric center are coincident, such that the force of gravity and the force of buoyancy act through the same point. As a result, the contributions to the force array due to the buoyancy of a completely submerged rigid body, free or constrained, are found in the same way as those for gravity, the only difference being the magnitude and direction of the buoyant force.

$${}^0_B(\vec{F}_{buoy})_i = \rho_f g V_i \hat{k}$$

where ρ_f is the density of the seawater and V_i is the volume of the rigid body.

This model of buoyancy as a constant force that depends only on the volume of a body and the density of the fluid is suitable only for fully submerged bodies. The buoyancy of surface penetrating features also depends on their position and orientation relative to the fluid surface, as well as the surface wave characteristics of the site. During the initial development of this program, surface penetrating systems are not considered. Several compliant-moored tidal turbine devices have been proposed with surface-penetrating features, therefore this functionality will be added in the future. Furthermore, it is likely that many real systems will involve structures with non-coincident centers of mass and buoyancy, and modifications will need to be made to account for that. The ability to define the location of the center of buoyancy of a fully submerged rigid body or to calculate the center of buoyancy of a surface-penetrating body as a function of that body's position and orientation will also be included in future versions of the program.

3.8.3. Fluid Forces

One of the greatest challenges of this project is the calculation of the fluid forces acting on the system. Due to the complex geometry of a tidal turbine and the structural compliance inherent in moored systems, the fluid forces and the fluid-structure interactions are difficult to model. As an initial attempt at solving these systems, the fluid forces are approximated component-wise as pure drag; that is, a given body will be subjected to drag forces calculated along its body-fixed axes, and a given line segment will be subjected to drag tangent and normal to its axis. This approach allows for the development of the program to a point where the governing equations of motion can be obtained and solved for using a reasonable approximation of fluid forces for simple geometries and light loading, however for the model to accurately simulate tidal turbine behavior in a sufficiently wide range of operating conditions, more

advanced calculations of the fluid forces to account for the effects of the rotating turbine blades, wake, flutter instabilities, turbulence, etc. will be needed.

3.8.3.1. Drag and lift

Figure 11 demonstrates how drag forces are decomposed into axis-aligned components and applied to a rigid body. In this figure, v_0 is the velocity of the fluid along the global y_0 -axis, v_1 and w_1 are the fluid velocities aligned to the body-fixed y_1 and z_1 axes, respectively, A_{y_1} and A_{z_1} are the body characteristic areas corresponding to flow along the y_1 and z_1 axes, respectively, and C_{D,y_1} and C_{D,z_1} are the coefficients of drag for fluid flow along the corresponding body-fixed axis.

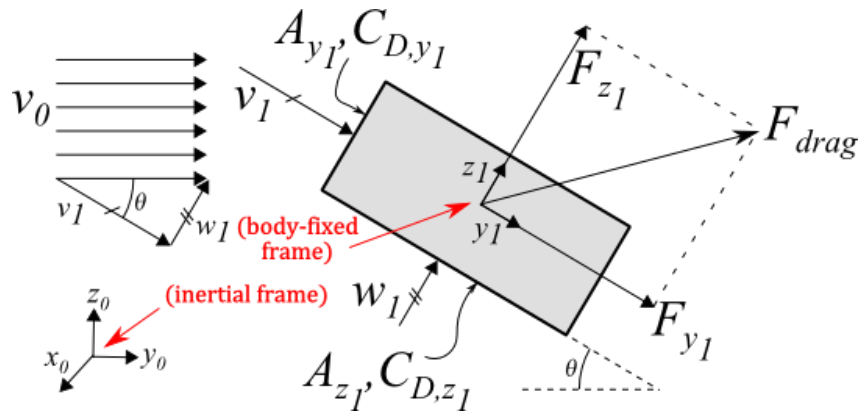


Figure 11: Component-wise drag calculation for rigid body

The drag forces on a rigid body are calculated component-wise using the equation

$$F_{drag,i} = \frac{1}{2} \rho_f C_{D,i} A_i u_i |u_i| \quad (29)$$

where $C_{D,i}$, A_i , and u_i are the coefficient of drag, characteristic area, and relative fluid velocity, respectively, with respect to the body-fixed coordinate i -direction, such that the total drag force vector is expressed in the body-fixed frame as ${}^B \vec{F}_{drag,i} = [F_{drag,x_i} \quad F_{drag,y_i} \quad F_{drag,z_i}]^T$. This force vector is then transformed to the inertial frame by multiplication with the body's direction cosine matrix and included in the force array e .

Many fluid flows of interest vary in space and are therefore non-uniform over a particular face of a rigid body; the velocity at the top of a face might be different than that at the bottom of the same face, and accounting for this variation would require integration of the fluid velocity over the area of the face in question. Rather than perform that integration, it is assumed that the fluid velocity variation over the face of a rigid body is small enough that its effect is negligible. Instead, the fluid velocity is taken as the quantity evaluated by plugging-in the coordinates of the center of mass of the body in the stream velocity function. This method is not suitable for utility-scale turbines since the large swept-diameter of such devices suggests that higher resolution of the flow velocity across the system boundary is needed.

Note that for geometries with values for the coefficients of drag and the characteristic areas that are equivalent along each direction (e.g. cube, sphere), the resultant drag force vector will always act parallel to the relative fluid flow regardless of body orientation. The assumption is made that most models will consist of geometries involving blunt objects that do not generate lift when their angle of attack with respect to the relative fluid flow is zero. In the case when the angle of attack is not zero, lift can potentially be developed when a body has differing values for its characteristic area or drag coefficient along each coordinate direction as a result of decomposing the relative fluid velocity into components aligned with each body-fixed axis, as demonstrated in Figure 11 by the fact that the resultant drag force is angled with respect to the relative fluid velocity. This indicates that there is both a vertical and horizontal component to the drag force, with the vertical component effectively amounting to a lift force. Future versions of this program will be able to accept tabulated values for lift and drag for a given body at various orientations to the relative fluid flow. This will allow for the inclusion of features such as hydrofoils in the system. Additionally, lift and drag forces obtained through experimentation of the actual body being used will undoubtedly be better than the approximations made using the drag force equation. Drag forces acting on rotating turbine blades could alternatively be

found through coupling of the mooring dynamics simulator with code utilizing blade-element-momentum theory to model the turbine.

Preliminary simulations are conducted by parameterizing the turbines as blunt objects, with a characteristic area given as the the “frontal area”, or the area of the turbine projected on a plane normal to the corresponding axis in the body-fixed frame. Since we are looking at the dynamics of the system and not just a steady state condition, the fluid velocity u cannot simply be taken as the free stream velocity, but rather the relative velocity between the rigid body and the free stream must be calculated. The relative velocity vector is found by subtracting the velocity of the body from the velocity of the fluid, then it is translated to the body-fixed frame by multiplication with the inverse of the Euler Angle direction cosine matrix derived in Section 3.3.1. With the relative velocity vector expressed as components along the body-fixed axes, the drag forces acting along those axes are found with equation (29). The drag force vector in the inertial frame is then found with another transformation using the direction cosine matrix.

To calculate the drag force on a constrained body, the velocity of the body expressed in the global frame is found from the velocity of its parent body using Equation (12). Once the drag force is calculated from Equation (29), it is translated to a force and moment couple using the same methods implemented to translate the gravitational force on a constrained body to its parent, as presented in Section 3.8.1.

The drag forces acting on the mooring lines are handled in a slightly different manner. Because the mooring line segments more closely resemble elongated cylinders rather than bluff bodies, the drag force experienced by a line segment is calculated as the vector sum of a tangential and normal force component, as shown in Figure 12. The tangential force component acts in a direction parallel to the line segment, whereas the normal force acts in a direction normal to the segment and in the plane created by the relative fluid velocity vector and the axis of the line segment, as shown in Figure 12. A

different strategy is needed for mooring lines with more complex geometries such as chains, whose segments do not resemble elongated cylinders. If the drag forces on a length of such a line in various fluid velocities and line orientations are known (either through experimentation or computerized hydrodynamic simulation) that data can be imported into the program which would then interpolate between data points to approximate the drag forces on a segment at any orientation and in a fluid stream at any velocity.

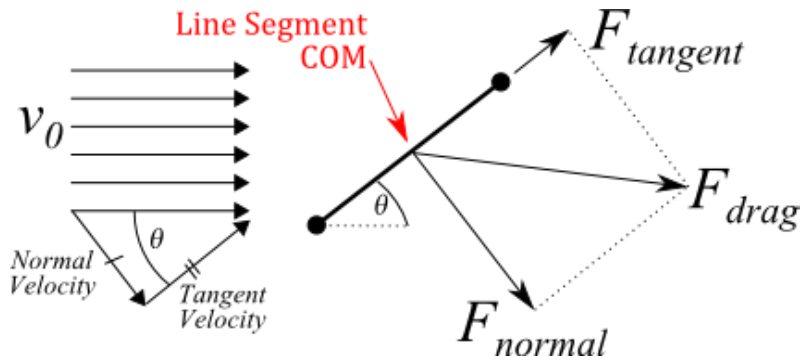


Figure 12: Drag Calculation for Line Segment

Using a lumped-parameter approach, the drag force on a line segment is calculated as though it is acting through the geometric center of the segment and then distributed evenly between the two adjacent line nodes. If one of those nodes is a line terminus, the drag force lumped to that node is handled in the same way as the gravitational force lumped to a line end-node. As for a rigid body, the relative fluid velocity is found by evaluating the free stream velocity at the line segment's center of mass, which is also its geometric center. Additionally, the line segment velocity is taken as the velocity of its geometric center, found as

$${}^0\vec{V}_i = \frac{1}{2}({}^0\vec{V}_i + {}^0\vec{V}_{i+1}) \quad (30)$$

$${}^0\vec{U}_{rel} = {}^0\vec{U}_{stream} - {}^0\vec{V}_i \quad (31)$$

where Line Segment i is the segment between Line Nodes i and $i + 1$. Next, the unit vector in a direction tangent to the line segment axis is calculated.

$$\hat{u}_{tan} = \frac{{}^0_{LN}\vec{P}_i - {}^0_{LN}\vec{P}_{i+1}}{\|{}^0_{LN}\vec{P}_i - {}^0_{LN}\vec{P}_{i+1}\|} \quad (32)$$

The magnitude of the relative fluid velocity in the direction tangent to the line segment is found as the dot product between the relative fluid velocity in the global frame and the unit vector in the tangent direction.

$$\|\vec{U}_{tan}\| = {}^0\vec{U}_{rel} \cdot \hat{u}_{tan} \quad (33)$$

Next, the magnitude of the relative fluid velocity component in the direction normal to the line is obtained as

$$\|\vec{U}_{norm}\| = \sqrt{\|{}^0\vec{U}_{rel}\|^2 - \|\vec{U}_{tan}\|^2} \quad (34)$$

Complex values for $\|\vec{U}_{norm}\|$ do not arise because the magnitude of the relative fluid velocity in the direction tangent to the line segment is always less than or equal to the magnitude of the total relative fluid velocity. The unit vector normal to the line segment and in the plane spanned by the tangential unit vector and the relative fluid velocity vector is found by

$$\hat{u}_{norm} = \frac{{}^0\vec{U}_{rel} - \|\vec{U}_{tan}\|\hat{u}_{tan}}{\|\vec{U}_{norm}\|}. \quad (35)$$

Next, the characteristic area corresponding to flow in the tangential and normal directions are calculated from the instantaneous segment length and the line diameter. The area used in the drag equation for calculating the tangential force component is the cylindrical surface area of the line segment, $A_{tan} = \pi d\ell$, where d is the line diameter (assumed to be constant under load) and ℓ is the instantaneous length of the line segment. For calculating the normal drag force component, the lengthwise projected area, $A_{norm} = d\ell$, is used. The instantaneous length is found from the position of the line nodes enclosing the segment.

$$l = \sqrt{({}_{LN}^0\vec{P}_{i+1} - {}_{LN}^0\vec{P}_i) \cdot ({}_{LN}^0\vec{P}_{i+1} - {}_{LN}^0\vec{P}_i)} \quad (36)$$

The resulting drag force vector is calculated as the sum of the tangential and normal drag forces acting on the segment:

$$\vec{F}_{drag} = \frac{1}{2}\rho_f C_{D,tan} A_{tan} \|\vec{U}_{tan}\|^2 \hat{u}_{tan} + \frac{1}{2}\rho_f C_{D,norm} A_{norm} \|\vec{U}_{norm}\|^2 \hat{u}_{norm} \quad (37)$$

This is the drag force acting on the center of mass of the uniform density line. The force is then distributed evenly to the line nodes enclosing the segment. The relevant force transformations are made if one of those nodes is a line terminus. In this manner, all terms in the drag force equation are known as symbolic functions of the independent displacement and velocity variables and added to the total force array e .

3.8.3.2. Added mass

Bluff bodies accelerating in a dense fluid such as sea water have to overcome not only their own inertia, but also that of the fluid they are displacing. This comes into play when deriving the equations of motion for a system in that the mass matrix must contain not just the mass of the body, but also what are called 'added mass' terms, which account for inertia of the fluid displaced by the body as it accelerates. The fluid inertia forces experienced by a cylindrical objects due to unbroken surface waves are described by Morison [21], whose investigations into this phenomenon revealed that the relative importance of fluid inertia forces depends on the ratio of the object's diameter length-scale to that of the wavelength of the surface waves. Added-mass inertia forces are most significant when the object length-scale is on a smaller order of magnitude than the wavelength, and are negligible when the object is large relative to the wavelength such that it acts as a section of wall.

When examining added mass inertia forces acting on bodies that are free to move in six degrees of freedom, the calculations for the kinetic energy of the system increase in complexity. Body

accelerations in one direction can potentially cause fluid inertia forces in multiple directions. The kinetic energy of the body-fluid system is therefore found as

$$T = \frac{1}{2} \bar{q}^T \bar{M} \bar{q} \quad (38)$$

Where \bar{q} is the 6x1 column vector of the body's independent velocity variables and \bar{M} is a 6x6 matrix containing the body mass and added mass inertia terms. The added mass terms needed to populate \bar{M} depend on the body's geometry and mass distribution and can be found in literature for simple geometries. For more complex (i.e. realistic) shapes, added mass parameters can be approximated by computational tools such as WAMIT, which provides added mass parameter values obtained from linear potential theory. Due to the added complexity associated with accounting for added mass inertia effects and the difficulty of validating such models, added mass effects are omitted from the simulation until such a time when results can be compared to experimental observations.

3.8.3.3. Vortex-induced motion

Vortices shed by a structure in a fluid flow exert forces on the structure acting perpendicular to the direction of flow. Under certain conditions, these forces excite oscillatory motion of the system on which they are acting. The frequency at which vortices are shed from fixed structures is related to the non-dimensional Strouhal number. For compliant structures in low speed flows, vortices are shed at the same frequency as that for fixed structures, however this relationship breaks down as the flow speed is increased and the shedding frequency approaches the vibration frequency of the structure. At these higher flow speeds, vortices are shed in sync with the oscillation of the structure. If these oscillations occur at a frequency near a dynamic resonant mode, significant motions may be observed.

It is important to include the effects of vortex-induced vibration in the dynamic model to ensure they do not result in undesired motion of the turbines or mooring elements. Unfortunately, vortex shedding is an inherently non-linear, multi-degree of freedom phenomenon that gives rise to complex forces that

make the dynamic response of a body difficult to model [22]. There has been some success by treating the system as a coupled wake-oscillator system (see [23]), however, to facilitate initial development of the current dynamic model, the effect of vortex-induced vibration is left to be added at a later stage.

3.8.4. Seafloor Impenetrability

The normal force exerted by the seafloor is modeled by a non-linear force applied to each z -displacement variable. The empirical form of the model is

$$\vec{F}_{Seafloor} = \frac{\eta}{z_i^2} \hat{k} \quad (39)$$

where η is a tuning variable (specified to within an order of magnitude) and z_i is the distance from the seafloor. In this way, the force is only significant when the displacement variable accounting for the z -position of a line node, free node, or rigid body is close to zero. The appropriate value of η depends on the length, mass, and number of discretized segments for a mooring line. This quantity should be chosen such that the normal force acting on the mooring line nodes due to the seafloor is in equilibrium with the gravitational and buoyant forces at an acceptably small distance from the seafloor. Larger values for η will cause the line to come to rest at unrealistically large distances from the seafloor, and values that are too small can lead to non-convergence as the denominator approaches zero. For a system with a submerged line segment weight equivalent of 1.5 kilograms, a value of $\eta = 10^{-3}$ produced realistic results.

This method does not take into consideration the physical dimensions of a rigid body. It is assumed that the desired information is whether a structural body collides with the seafloor or not, rather than how the system responds when it does. On the other hand, the response of a system with mooring-line interaction with the seafloor is of interest, and this model gives a reasonable representation of mooring-lines lying partially on the seafloor.

3.8.5. Applied Forces

Additional forces can be directly applied to any rigid body as functions of time and body displacement. These forces can be defined in either the inertial frame or the body-fixed frame. Defining a force in the inertial frame means that the force will act in a given direction regardless of the orientation of the rigid body. An example of how this functionality can be utilized is to model active buoyancy control, wherein the buoyancy of a body changes with its position above the seafloor, since the buoyant force always acts in the inertial z-direction. An applied force defined with respect to the body-fixed frame is useful for modeling thrust or a reaction torque experienced by a rotating turbine, since the directions in which these forces act are dependent on the orientation of the body. Applied forces can be used to develop active or passive control strategies for turbine positioning and orientation.

3.9. Numerical Solution

To carry out the differentiations described by Lagrange's Equation of Motion, the function *diff.m*, which is built into the MATLAB Symbolic Math Toolbox, is utilized within a script to automatically derive the system of equations based on the expressions obtained for the kinetic, potential, and dissipated energies of the system, as well as the expressions for the net force acting on each element.

Once the system of governing equations is assembled, it is solved based on the user-defined initial conditions using a built-in implicit numerical integration function called *ode15i.m*. This implicit method is chosen since it is expected that an explicit method, one where the state at a given time-step depends solely on the state at the previous time step, would be numerically unstable due to the high expected stiffness of many turbine mooring systems. Solving the system of differential equations which govern the model yields numerical values for every displacement variable in the system, which corresponds to an x , y , or z position for all unconstrained rigid bodies, free nodes, and line nodes, as well as an α , β , γ Euler angle rotation for the rigid bodies, at each time step. This data helps to create a

visual and statistical representation of how the system is expected to behave and can be used to determine other characteristics of the dynamic response of the system to a given fluid flow field.

4. Model Validation

4.1. Steady State Systems

A simple way to verify whether the numerical results mirror real systems is to compare the results of the static equivalent to a dynamic system (or a steady-state solution) to analytical expressions of the system. Three such comparisons are made, one involving a simple elastic catenary, another composed of a cable with fixed end-points and a single force applied to the cable, and the last which makes use of results of equilibrium models of compliant-moored tidal turbines developed at an earlier stage of this project.

4.1.1. Elastic catenary

The first benchmark test was carried out with a simple elastic catenary model run until a steady state condition was reached. An analytical solution to this problem was developed by Irvine [24] and rewritten by Raman-Nair & Baddour [25] for the geometry shown in Figure 13.

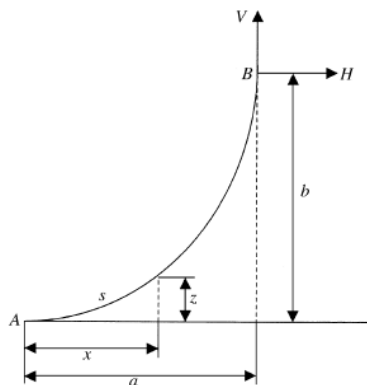


Figure 13: Elastic catenary benchmark test geometry

The analytical solution gives expressions for the x - and z -coordinates of the line at a length s along its un-stretched equivalent arc-length.

$$x(s) = \frac{Hs}{EA_0} + \frac{H}{\rho_b g} \left[\sinh^{-1} \left(\frac{V - \rho_b g L_0 + \rho_b g s}{H} \right) - \sinh^{-1} \left(\frac{V - \rho_b g L_0}{H} \right) \right],$$

$$z(s) = \frac{s}{EA_0} \left(V - \rho_b g L_0 + \frac{1}{2} \rho_b g s \right) + \frac{H}{\rho_b g} \left\{ \left[1 + \left(\frac{V - \rho_b g L_0 + \rho_b g s}{H} \right)^2 \right]^{\frac{1}{2}} - \left[1 + \left(\frac{V - \rho_b g L_0}{H} \right)^2 \right]^{\frac{1}{2}} \right\}.$$

In these expressions, H and V are the applied horizontal and vertical forces, respectively, acting on the free end of the cable, E is the modulus of elasticity of the cable, A_0 is the cross-sectional area, $\rho_b g$ is the submerged cable weight per unit length, and L_0 is the un-stretched length of the cable. The distances a and b are found by setting $s = L_0$.

It should be noted that this system does not include drag forces. The line is subjected to applied loads at the free end and to gravity only. For this reason, drag is omitted from the dynamic model by setting all drag coefficients to zero. Additionally, this test validates a steady-state solution to a dynamic problem. At steady state, the kinetic energy of the system drops to zero and all that remains is the potential energy in the system due to the elasticity of the mooring lines. Therefore, this serves as a validation case for the representation of potential energy in the system.

To compare the methods presented here to this analytical solution, a model similar to that used by Raman-Nair & Baddour was constructed. This model consists of a solid spherical buoy of radius $a_0 = 1 \text{ m}$ and density $\rho_0 = 800 \text{ kg/m}^3$ with a single line attached to its center of mass. The line has diameter $d_0 = 35 \text{ mm}$, the corresponding cross-sectional area $A_0 = 9.621 \times 10^{-4} \text{ m}^2$, mass per unit of un-stretched length $\rho = 50 \text{ kg/m}$, un-stretched length $L_0 = 13 \text{ m}$, and modulus of elasticity $E = 10^7 \text{ N/m}^2$. A constant horizontal force of $H = 1000 \text{ N}$ is applied to the center of the buoy. The applied vertical force is calculated as the difference between the gravitational force and the force due to

buoyancy to which the buoy is subjected, which is calculated from the volume of the buoy, its density, and the density of the water displaced by the buoy to be

$$V = (\rho_f - \rho_0) \left(\frac{4}{3} \pi a_0^3 \right) g = (1000 - 800) \frac{kg}{m^3} \left(\frac{4}{3} \pi 1^3 m^3 \right) 9.81 \frac{m}{s^2} = 8218.4 N$$

where ρ_f is the fluid density (which is assumed to be fresh water with $\rho_f = 1000 \frac{kg}{m^3}$).

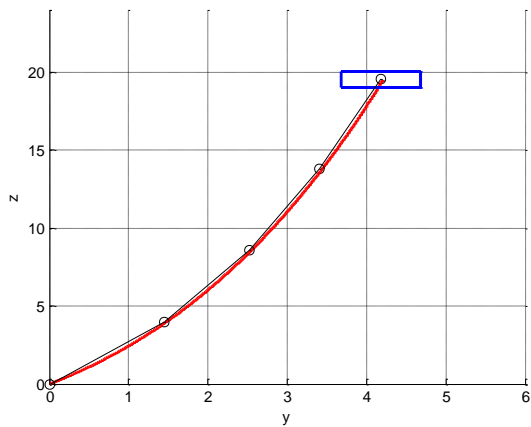
The submerged cable weight per unit length is calculated from the linear mass density of the cable, its volume, and the density of the fluid to be

$$\rho_b = \rho - \rho_f A_0 = 50 \frac{kg}{m} - \left(1000 \frac{kg}{m^3} \right) (9.621 \times 10^{-4} m^2) = 49.04 \frac{kg}{m}$$

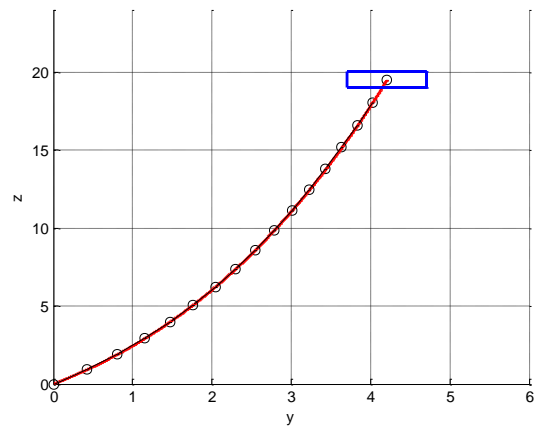
The test was carried out by configuring a system using the numerical program such that the user input parameters generate an identical system to that described above. Since this analytical solution applies to the steady-state condition, any initial position can be chosen as long as the model is run until the steady-state condition is reached. The horizontal and vertical forces at the free end of the line are applied directly in the system configuration file. To model the un-stretched length of 13 meters, the anchor point was set to (0,0,0), the initial displacement of the rigid body was set to (0,0,13), and the cable attachment point on the rigid body was set to the body's origin, (0,0,0) in the body-fixed frame. To model the modulus of elasticity of $10^7 N/m^2$, the unit length spring constant is calculated to be

$$k_{unit} = k_{total} L = \frac{EA}{L} L = EA = \left(10^7 \frac{N}{m^2} \right) (9.621 \times 10^{-4} m^2) = 9621 \frac{Nm}{m}$$

These values are entered into the system configuration file with a varying number of line segments in order to see how the profile of the weighted mooring line subject to gravity and defined loads at its free end compares to the analytical solution developed by Irvine. Figure 14(a) shows the solution obtained using four line segments compared to the analytical solution and Figure 14(b) shows the solution obtained using sixty-four line segments compared to the analytical solution.



(a) Numerical solution for 4 line segments



(b) Numerical solution for 16 line segments

Figure 14: Elastic Catenary – Numerical solution (black line with data points indicated by 'o') overlaid on analytical solution (red curve)

Error is calculated as the length of the vector from the line nodes of the numerical solution to the position found using the analytical expressions at the corresponding arc-length for a given node. Figure 15 shows that as the number of segments increases exponentially, the line profile obtained from the numerical solution more closely matches that of the analytical solution until the number of line segments becomes too large and finite precision round-off errors begin to dominate.

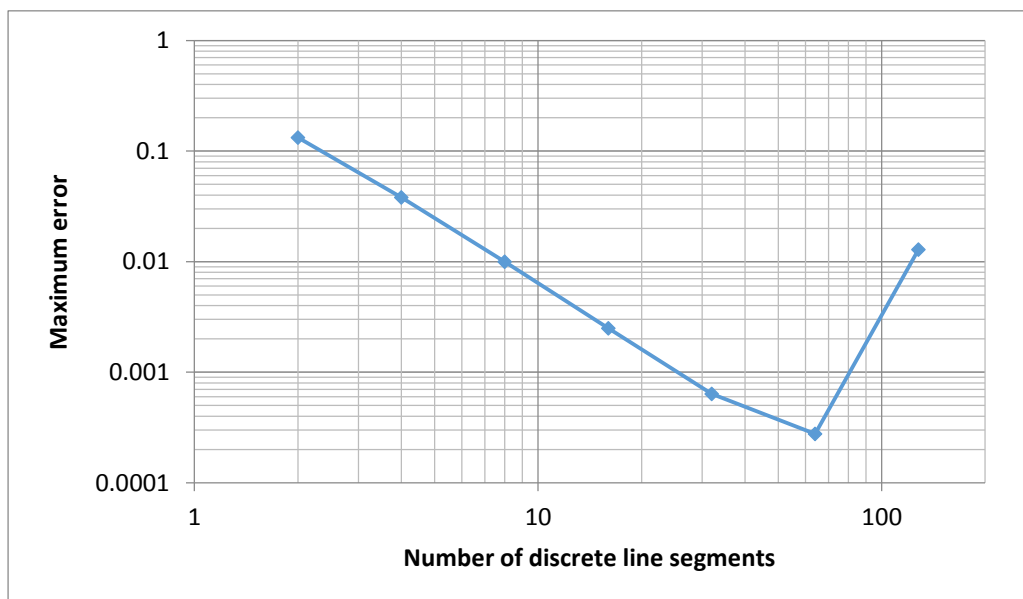


Figure 15: Maximum error of numerical solution as a function of increasing number of line segments

4.1.2. Point-mass on line with fixed end points

The second benchmark test to validate steady-state solutions involved a cable suspended between two fixed points with a point mass applied at some length along the cable, as depicted in Figure 16.

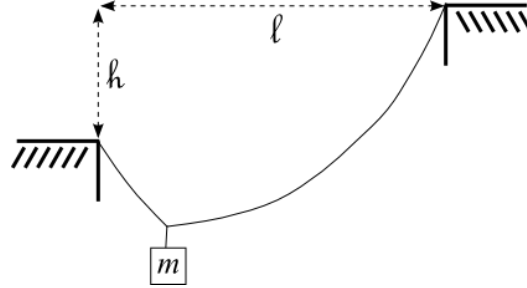


Figure 16: Point mass on line with fixed end points

The y and z coordinates of the centerline of the cable were derived analytically as functions of the unstretched equivalent arc-length s by Irvine [24] to be

$$y(0 \leq s \leq s_1) = \frac{Hs}{EA_0} + \frac{HL_0}{W} \left[\sin^{-1} \left(\frac{V}{H} \right) - \sin^{-1} \left(\frac{V}{H} - \frac{Ws}{HL_0} \right) \right];$$

$$y(s_1 \leq s \leq L_0) = \frac{Hs}{EA_0} + \frac{HL_0}{W} \left[\sin^{-1} \left(\frac{V}{H} \right) - \sin^{-1} \left(\frac{V - F_1}{H} - \frac{Ws}{HL_0} \right) + \sin^{-1} \left(\frac{V - F_1}{H} - \frac{Ws_1}{HL_0} \right) - \sin^{-1} \left(\frac{V}{H} - \frac{Ws_1}{HL_0} \right) \right];$$

$$z(0 \leq s \leq s_1) = \frac{Ws}{EA_0} \left(\frac{s}{2L_0} - \frac{V}{W} \right) - \frac{HL_0}{W} \left[\left(1 + \left(\frac{V}{H} \right)^2 \right)^{\frac{1}{2}} - \left(1 + \left(\frac{V}{H} - \frac{Ws}{HL_0} \right)^2 \right)^{\frac{1}{2}} \right];$$

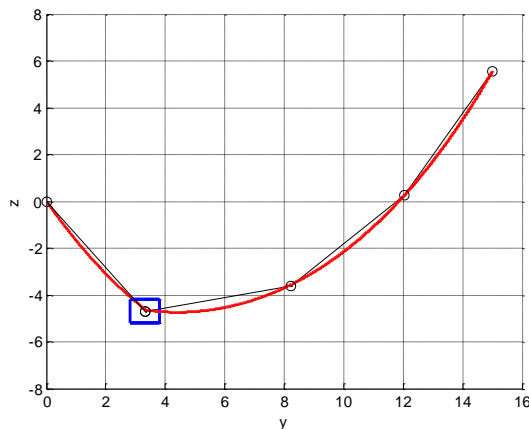
$$\begin{aligned}
z(s_1 \leq s \leq L_0) = & \frac{Ws}{EA_0} \left(\frac{s}{2L_0} - \frac{V}{W} \right) \\
& - \frac{HL_0}{W} \left[\left(1 + \left(\frac{V}{H} \right)^2 \right)^{\frac{1}{2}} - \left(1 + \left(\frac{V - F_1}{H} - \frac{Ws}{HL_0} \right)^2 \right)^{\frac{1}{2}} + \frac{F_1 W}{HEA_0} \left(\frac{s_1}{L_0} - \frac{s}{L_0} \right) \right. \\
& \left. + \left(1 + \left(\frac{V - F_1}{H} - \frac{Ws_1}{HL_0} \right)^2 \right)^{\frac{1}{2}} - \left(1 + \left(\frac{V}{H} - \frac{Ws}{HL_0} \right)^2 \right)^{\frac{1}{2}} \right].
\end{aligned}$$

In these equations, H and V are analogous to the horizontal and vertical applied forces from the elastic catenary benchmark problem discussed in Section 4.1.1, however since the end point in this case is fixed, H and V are better described as reaction forces to the weight of the cable and the point load. The values for H and V are therefore obtained from the above equations by setting $y = \ell$ and $z = h$ at $s = L_0$, where ℓ and h are the horizontal and vertical distances from one fixed-end to the other. The point load F_1 is applied at $s = s_1$ and acts solely in the vertical direction. In the above equations, F_1 is positive when the force acts in the negative z -direction.

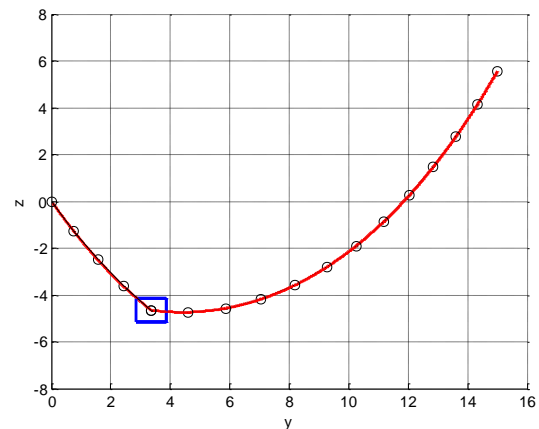
For this benchmark test, a model was generated with a cable of un-stretched length $L_0 = 16 \text{ m}$ and end points at $(x, y, z) = (0,0,0)$ and $(0,15,5.568)$. The point load was chosen to be due to a 1 meter radius sphere with a density of 1050 kg/m^3 and corresponding mass of 4398 kg . The cable and sphere are submerged in fresh water with a density of 1000 kg/m^3 . The value of the point load F_1 is therefore calculated to be $F_1 = (1050 - 1000)(\text{kg/m}^3)(4\pi/3)(1 \text{ m})^3(9.81 \text{ m/s}^2) = 8218.4 \text{ N}$ acting downwards. The cable has a modulus of elasticity $E = 10^7 \text{ Pa}$, a diameter of 35 mm, and a linear density of 50 kg/m . The value for the cable self-weight W in the above equations is calculated as $W = (50 \text{ kg/m})(9.81 \text{ m/s}^2)(16 \text{ m}) = 7848 \text{ N}$ and the cable cross-sectional area $A_0 = \frac{\pi}{4}(0.035 \text{ m})^2 = 9.621(10^{-4}) \text{ m}^2$.

The analytical solution was obtained using the above values in the equations given to find the y - and z -components of the cable position at an arc-length s along the cable. The values for H and V were found

by solving the equations at $s = L_0 = 16 \text{ m}$. Since it is known that at this arc-length, $y = 15 \text{ m}$ and $z = 5.568 \text{ m}$, the only unknowns are H and V and the system of two equations and two unknowns is easily solved. The numerical solution is obtained using the methods discussed in this paper and running the simulation until a steady-state condition is reached. The time required to reach steady-state depends on the values entered for the drag coefficients and/or damping coefficients, however so long as these values are greater than zero, the same steady-state solution will be reached. Figure 17(a) shows the numerical solution obtained using four line segments overlaid on the analytical solution. Figure 17(b) shows the results obtained when the number of line segments is increased to sixteen. These figures show that the numerical results are in very close agreement to the analytical solution even when the number of line segments is small.



(a) Numerical solution for 4 line segments



(b) Numerical solution for 16 line segments

Figure 17: Fixed end-points with single point-mass – Numerical solution (black line with data points indicated by 'o') overlaid on analytical solution (red curve)

These results indicate that the static-equivalent solutions obtained by the numerical dynamic model are in good agreement with results obtained from analytical cable methods. The consistency between the numerical and analytical models serves as evidence that these methods yield accurate representations of the potential energy and spring forces in the system. However, since the first two benchmark tests

involved systems without a fluid flow, they tell us nothing about the model for drag forces that was adopted for the program. This model will be validated in the next benchmark test.

4.1.3. Comparison to Steady-State Tidal Turbine Equilibrium Model

The final steady-state benchmark test evaluates the equilibrium position of a potential tidal turbine system. The results obtained by running the dynamic model until a steady-state condition is reached are compared to results of an equilibrium model developed by DuBuque [26], who presents a numerical method to obtain the equilibrium position of a tidal turbine in a steady fluid flow through iterative minimization of the potential energy of the system. The system configuration selected is shown in Figure 18.

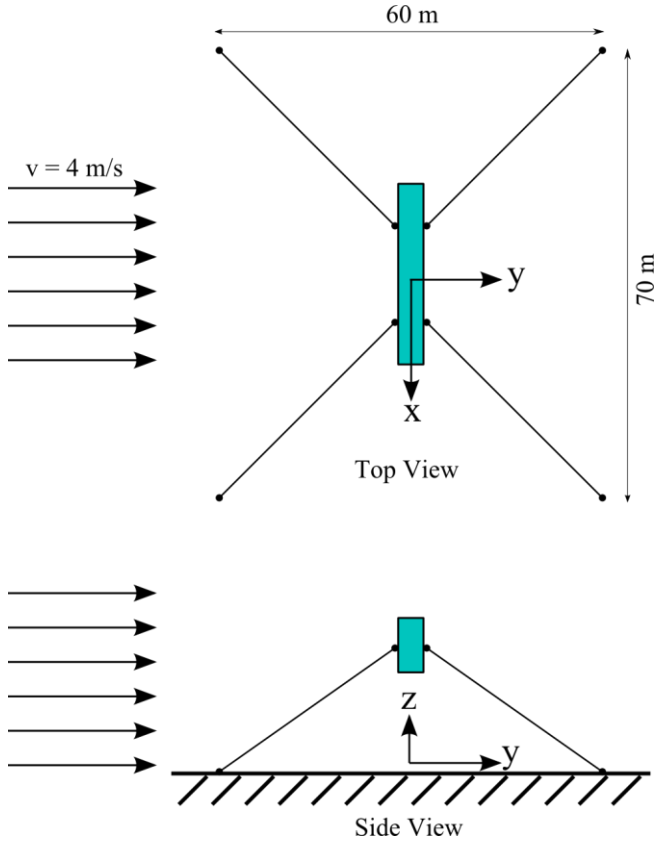


Figure 18: System schematic for comparison to static-equilibrium model

This system is composed of a single rigid body with four mooring lines in a fluid with density $\rho = 1020 \text{ kg/m}^3$ moving with a uniform velocity of 4 m/s. The body measures 28 m wide, 4 m deep, and 8.5 m tall. Due to the fact that this body represents a tidal turbine which allows some fluid to pass through its volume, the effective surface areas of the body are only a small percentage of the total rectangular surface area. The rigid body properties for this system are given in Table 1.

Table 1: Static comparison benchmark test - Rigid body properties

Property	Value
Mass:	$m = 5000 \text{ kg}$
Moment of Inertia:	$I = [I_{x_1} \quad I_{y_1} \quad I_{z_1}] = [4 \quad 4 \quad 4] \text{ kg m}^2$
Volume:	$V = 10 \text{ m}^3$
Initial position in global frame:	$Y_0 = [x_0 \quad y_0 \quad z_0] = [0 \quad 0 \quad 20] \text{ m}$
Initial orientation in global frame:	$\theta_0 = [\alpha_0 \quad \beta_0 \quad \gamma_0] = [0 \quad 0 \quad 0] \text{ rad}$
Characteristic (projected) Area:	$A = [A_{x_1} \quad A_{y_1} \quad A_{z_1}] = [16 \quad 24 \quad 11] \text{ m}^2$
Coefficients of drag:	$C_D = [C_{D,x_1} \quad C_{D,y_1} \quad C_{D,z_1}] = [0.5 \quad 0.5 \quad 0.5]$

The mooring line stiffness is based on a material with a Young's modulus of 10 GPa and a diameter of 5 cm. The resulting unit spring constant is found to be

$$k_{unit} = EA = \left(10 \times 10^9 \text{ N/m}^2\right) \frac{\pi}{4} (0.05 \text{ m})^2 = 19635000 \text{ (N/m)m}$$

This is the spring constant for a line 1 meter in length. The program uses this value to calculate the spring constant for each line segment based on the length of each segment, which is determined by the overall length of the mooring line and the number of segments into which it is divided as stipulated by the user. The remaining mooring line properties are presented in Table 2.

Table 2: Static comparison benchmark test – Mooring line properties

Property	Value
Linear mass:	$m = 10 \text{ kg/m}$
Diameter:	$d = 0.05 \text{ m}$
Length:	$L = 44 \text{ m}$
Unit stiffness:	$k_{unit} = 19635000 \text{ (N/m)m}$
Coefficients of drag:	$C_D = [C_{D,tan} \ C_{D,norm}] = [0.05 \ 0.05] \text{ m}$

The simulation is run for a long enough duration such that the system reaches steady-state. The resulting equilibrium position and orientation of the rigid body are presented in Table 3, along with those observed by DuBuque for comparison.

Table 3: Static comparison benchmark test - Results

Position/Orientation	Static Model [26]	Dynamic Model	Error
$x \text{ (m)}$	10^{-5}	0	0%
$y \text{ (m)}$	2.263	2.3864	5%
$z \text{ (m)}$	16.30	16.0411	1.6%
$\alpha \text{ (rad)}$	0.3809	0.3758	1.3%
$\beta \text{ (rad)}$	10^{-6}	0.0	0%
$\gamma \text{ (rad)}$	10^{-6}	0.0	0%

Figure 19 shows the resulting static-equilibrium position of the rigid body and line nodes as given by the dynamic model. This closely matches the equilibrium state of the system as found from the static model developed by DuBuque, which is shown in Figure 20.

The validity of the model for drag forces acting on a rigid body and mooring line system under steady state conditions is evidenced by the consistency between the static-equilibrium model and the static-equivalence obtained from the dynamic solution.

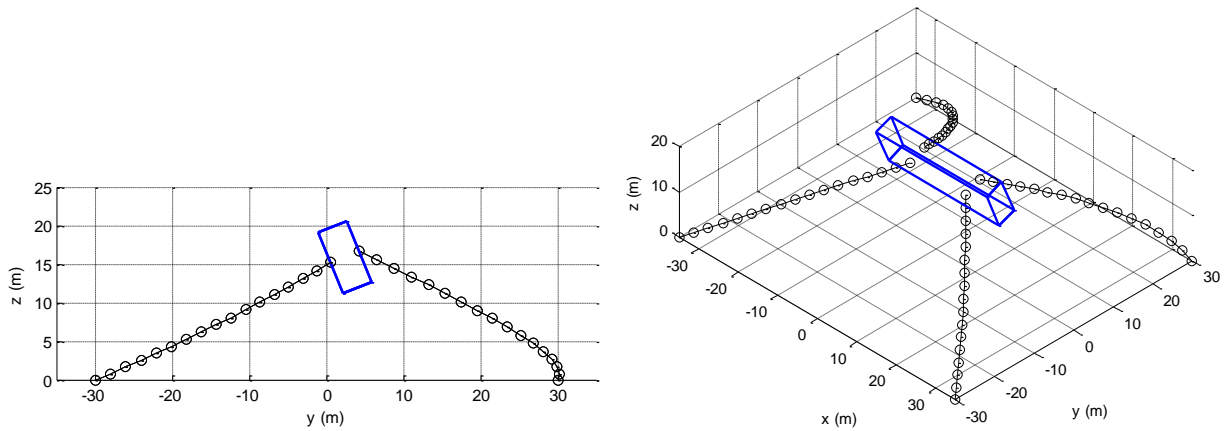


Figure 19: Static-equilibrium obtained from dynamic model

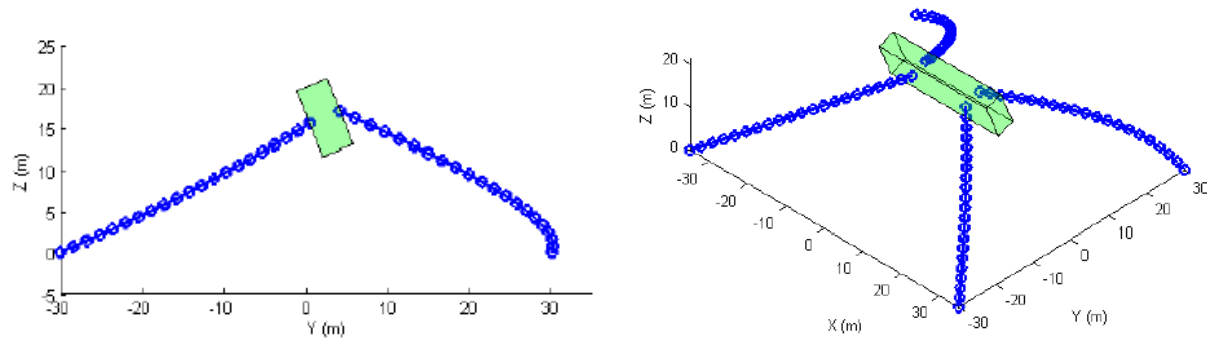


Figure 20: Equilibrium position obtained from static model [26]

4.2. Dynamic Systems

The steady-state benchmark tests show that the numerical methods employed here yield reasonable results when the only forces acting on the system are spring forces, gravity/buoyancy, and drag.

Knowing this, we can move on to assess the validity of the kinetic energy model of the system. This cannot be done with comparisons to steady-state conditions, therefore the following test case deals with the motion exhibited by a system subjected to various forces in the time-domain. The results of this test will reveal how well the program accounts for changes in the kinetic energy of the system and how that relates to the system dynamics.

4.2.1. Mass-Spring-Damper system

The first dynamic validation test is used to determine the efficacy of the automatic derivation and solution of the equations of motion of a system without consideration to the developed fluid forcing models. For this test, a two degree of freedom mass-spring-damper system is modeled and the behavior as obtained from the numerical model is compared to the analytical solution to the governing equations of motion. The chosen test system is presented in Figure 21(a). Careful attention must be paid to ensure that the system generated in the numerical model accurately resembles the chosen test system due to the fact that the numerical model expects all compliant lines to be continuous with uniform linear mass, whereas the test system utilizes ideal massless springs. Similarity is achieved in the numerical model by describing a system with a single mooring line discretized into two segments attached to a rigid body. By dividing the mooring line into only two segments, a single lumped-parameter line node is created which is analogous to mass 2 in the test system. The lumped-mass of the sole line node is equal to the mass of one line segment; additionally, a quantity of mass equal to one-half that of the line segment mass is lumped to the rigid body as part of the discretization scheme, therefore the linear mass of the mooring line and the mass of the rigid body must be chosen such that the resulting lumped-masses of the line node and rigid body are equal to the masses m_1 and m_2 in the test system, respectively. The unit spring constant of the mooring lines must be chosen such that the resulting spring constant of each line segment is equal to the spring constant k in the test system. Buoyant forces are omitted from this test.

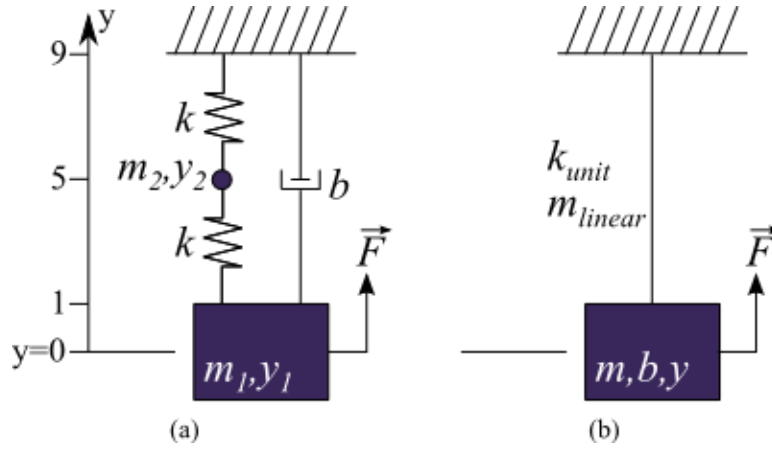


Figure 21: Mass-Spring-Damper system for first dynamic validation test

In the test system, the body masses m_1 and m_2 are set to 100 kg and 8 kg respectively, the spring constants of both springs are set to 500 N/m, and the damping constant is set to 10 Ns/m. A sinusoidal force is applied as a function $\vec{F} = -500N \sin(2\pi t/(10s))$. The governing equations of motion for this system are expressed as

$$m_1 \ddot{y}_1 = -m_1 g + k(y_2 - y_1 - 5m) - b \dot{y}_1 - 500N \sin(2\pi t/(10s))$$

$$m_2 \ddot{y}_2 = -m_2 g + k(5m - y_2) - k(y_2 - y_1 - 5m)$$

With the initial positions of each mass as shown in the figure and the initial velocities of both masses set to zero, this system of differential equations of motion is easily solved analytically using Mathematica to obtain the vertical position of masses m_1 and m_2 as functions of time.

The corresponding system as modeled in the dynamic modeling program is shown in Figure 21(b), where the mooring line is modeled as two discrete 4 meter segments. To match the test model, the unit spring constant is set to $k_{unit} = (500 \text{ N/m})(4m) = 2000 \text{ Nm/m}$. The linear mass is set to 2 kg/m such that the mass of the lumped-parameter node is 8 kg, and the mass of the rigid body is set to 96 kg so when the mass of half of a line segment is lumped to the body, the result is equal to m_1 . Because the damper

in the test system acts between body 1 and the fixed inertial frame, its value is the same as that applied to the rigid body in the dynamic model.

The simulation is run several times while varying the value for the relative and absolute error tolerance applied to the ODE solver. Figure 22 shows the resulting maximum error between the solution (y-position of the mass as a function of time) obtained analytically and that found by our numerical method as a function of the solver tolerance. The figure demonstrates that as the tolerances are tightened on a logarithmic scale, the absolute error between the analytical and the numerical solutions also decreases logarithmically.

This test serves to validate several key components of the program. It shows that the program is able to effectively extract the differential equations of motion of a system involving a mass, a flexible cable, and a damper. Additionally, the results prove that the ODE solver is capable of solving the equations of motion and producing a representation of the system behavior with an accuracy dependent on the specified error tolerance. This test was conducted with only two discretized line segments so that an analytical solution to an equivalent system could easily be found. The results allow the conclusion to be drawn that as the number of line segments is increased, the model will better reflect the behavior of a mass tethered by a continuous flexible mooring line with uniform linear mass and stiffness. What this test does not validate is the fluid forcing model, since fluid forces were not applied. Further testing is required in order to determine whether the fluid force model accurately approximates the forces to which a body is subjected due to motion relative to a fluid flow.

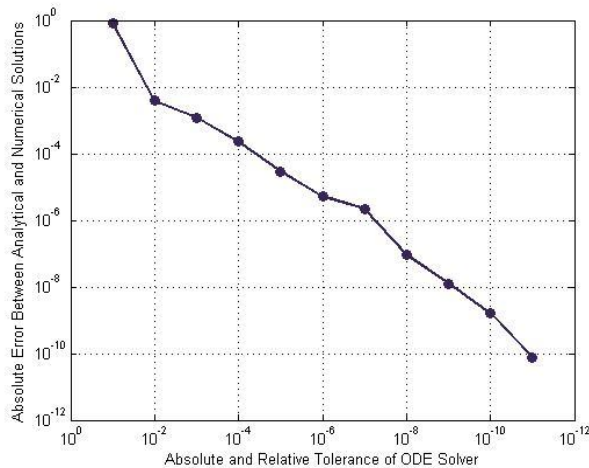


Figure 22: Error as a function of ODE Solver tolerances

5. Future work

A great deal of effort is still required to advance the dynamic numerical simulation to the point where it can reasonably model real-world moored tidal turbine systems. Most of this effort will be applied to refining the fluid loading model. Fluid forces arise from drag, added mass effects, turbulence, and oscillatory wave motion in a manner more complicated than what can be modeled with a single non-linear drag representation. The results of the validation tests described within this paper provide confidence that the algorithm employed to develop the Lagrangian differential equations of motion for a given mooring-line/submerged-body system are likely to yield satisfactory results when taking into account the gravitational, buoyant, and non-linear drag forces acting on the system. This method of solving for the equations of motion differs from existing mooring models in that it allows for full three-dimensional translation and rotation of the solid bodies.

Features such as non-coincident centers of mass, buoyancy, and drag pressure, as well as surface penetration and surface wave loading are in the process of being incorporated into the model. The greatest challenge, at present, is addressing more stochastic fluid loading effects resulting from turbulence, flutter instabilities, fluid-structure interaction, as well as the effects of energy extraction by

the turbine. Development of methods to capture these effects will be a major focus of ongoing research, though it is possible that no universally applicable model will be available.

5.1. Turbulence Modelling and Dynamic Comparison

Most flows suitable for tidal energy harvesting will possess inherent turbulence as a result of site-specific bathymetry and geophysical features. For a dynamic model to accurately represent the response of a compliant-moored system to the expected flow characteristics, this turbulence must be accounted for. This can be achieved through statistical analysis of turbulence, wherein a value of turbulence intensity is defined as the ratio of turbulent fluctuations to the mean flow velocity. The value for the turbulent fluctuations is typically taken as the standard deviation of the flow speed, such that $I_u = \sigma_u / \bar{u}$. With this metric, turbulent flows can be realized numerically by defining a mean velocity, constant or a function of time and space, as well as the turbulence intensity and the frequency spectra in which the fluctuations might occur. A flow profile is then generated making use of a random number generator to assist in creating intermittent coherent structures within the flow field to represent turbulent fluctuations from the mean fluid velocity, such that the resulting turbulence intensity matches the defined value. Measured turbulence intensities from various tidal energy sites are around 10% [16], which is consistent with measurements from wind energy site studies and serves as a good default value if no measurements of turbulence at a specific site are available. However, the best results will be obtained by measuring the turbulence intensity at the proposed tidal turbine deployment site.

Including turbulent effects in the numerical model is important as it reveals dynamic system behavior related to the structural resonance of the system. Knowledge of the resonant modes of a particular mooring design will help developers ensure that the existence of such modes does not interfere with the operation of the device.

5.1.1. Dynamic Comparison to TTM Deployment

The success of this project depends on our ability to prove the program yields realistic results. Therefore, validation against real data from instrument deployments is necessary. The first fully dynamic comparison to a real system will be made using data collected by a Tidal Turbulence Mooring (TTM) device which was deployed in Admiralty Inlet, Washington State, in 2012 [17], shown in Figure 23.

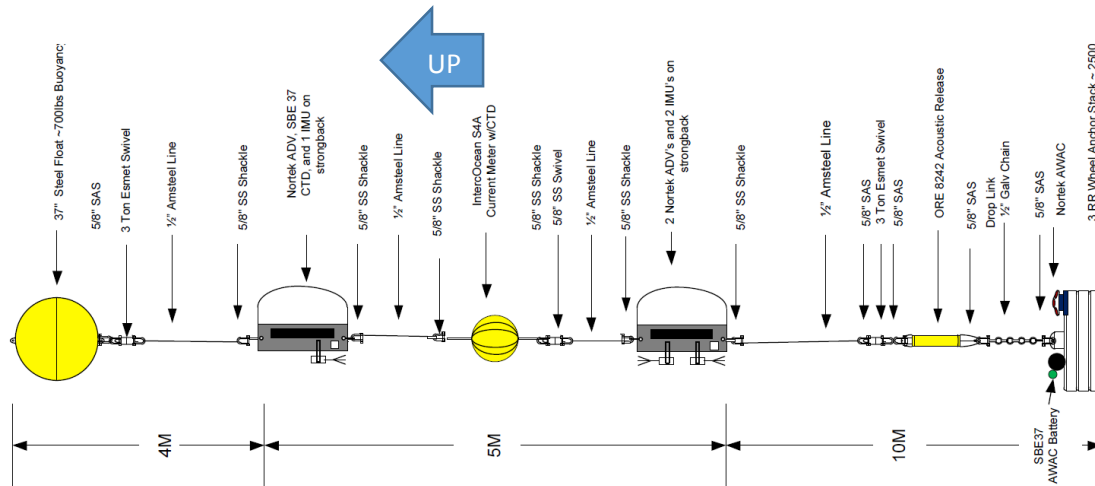


Figure 23: Tidal Turbulence Mooring data collection instrument

Two tests are planned: The first uses a time-domain fluid velocity input including turbulent fluctuations, which is obtained from the motion-corrected ADV data collected during the deployment. This will be used in a direct motion comparison between the dynamic response given by the numerical simulation and the actual observed motion of the mooring. The second test will use a statistical representation of the turbulent flow using the turbulence intensity metric described above. The comparison will be made between the observed mooring acceleration spectra, shown in Figure 24, and the spectra obtained through numerical modelling. Specifically, we will look for similarities in the appearance of a resonant mode at lower mean fluid velocities, as evidenced in Figure 24. Consistent results between the numerical solution and observed behavior would validate the functionality of this program as a tool for simulating the dynamic response of a proposed tidal turbine mooring configuration to turbulent flow.

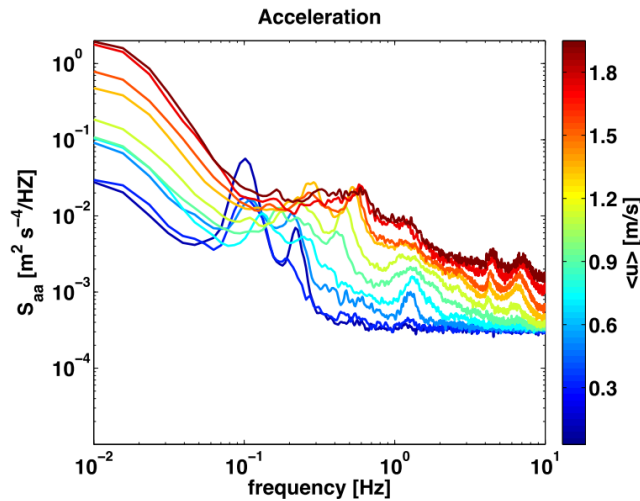


Figure 24: Acceleration Spectra of TTM response to turbulent flow [17]

5.2. Initialize to equilibrium

When a system is assembled, the program currently takes the position values defined by the user to create the system as the initial position values of the simulation. This means that, in steady and unsteady flows, there will be a transient response of the system dynamics to these out-of-equilibrium starting positions as the forces of gravity, buoyancy, drag, and line tension come into balance. This transient response typically is an undesired artifact of the way a system is set up in the program, since it is unlikely that a real system would be held at a specified position and suddenly released.

Therefore, the code must be modified such that the initial position of the bodies and nodes are in static equilibrium under the instantaneous initial fluid velocity. This will eliminate the undesired transient response of the system to the initial positions used to define the system configuration, thereby allowing useful results to be taken from the full duration of the simulation. The equilibrium starting position will be calculated prior to solving the equations of motion through iterative minimization of the potential energy of the system following the techniques developed by DuBuque [26].

5.3. Collaboration

The need to validate these methods against real-world data presents the opportunity for collaboration with groups in possession of this type of data and interested in a full-range-of-motion dynamic model for a system within the scope of our applications. The program can serve to provide insight into the way changes to a system design would impact the overall system behavior and performance, allowing designers to assess the impact of design changes prior to expending the cost and effort of applying those changes. One group that has expressed interest in using this development tool is the Center for Ocean Renewable Energy at the University of New Hampshire, which has been investigating the dynamic behavior of a floating platform-mounted hydrokinetic turbine and mooring system, the basic configuration of which is presented in Figure 25.

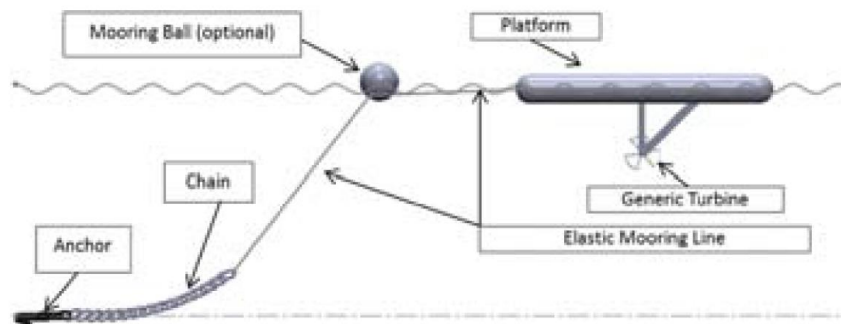


Figure 25: UNH barge-mounted hydrokinetic turbine [27]

Data collected from a deployment of this test system in Muskeget Channel in July of 2012 measures the surge, heave, and pitch of the barge when subject to a steady current and to surface waves characterized by a significant wave height and peak wave frequency. Figure 26 shows the measured spectral response of the barge to waves of a given radian frequency in flow characterized by a bulk fluid velocity of 1.9 m/s and significant wave height of 0.5 m . Also included in the figure are the values predicted by UNH using both a single frequency wave model from linear wave theory as well as a random frequency wave model.

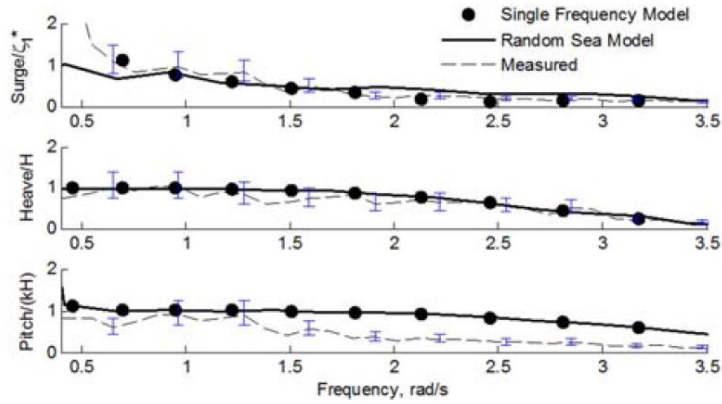


Figure 26: Measured response of barge to fluid loading compared to UNH predictions

The equations developed by UNH to model this system produce results that match reasonably well with the observed behavior of the barge, however, they were developed specifically for this system and as such would require careful modification to apply to a system with added features or significant design changes. Once functionality for surface wave modeling is included in the program described in this paper, the UNH barge-mounted turbine system, as well as a wide range of other surface-penetrating or fully submerged systems, can be modeled without the need to manually derive a new set of governing equations of motion. Through collaboration with the University of New Hampshire, the predicted dynamic behavior obtained through modeling of the UNH barge system in the program described herein will be compared to the data collected from ocean deployments. This will allow for improvements to be made to the program and serve to further validate these methods and demonstrate the utility of this program to the marine renewable energy community.

6. Conclusion

A numerical method of solving for the dynamic behavior of compliant-moored systems in fluid flow was presented in this paper. A system is described as an assemblage of mooring lines and rigid bodies. Expressions for the total kinetic, potential, and dissipated energy as functions of the displacements and velocities of each system feature are found computationally based on the system description defined by the user. The relevant forces acting on the system are also expressed as functions of displacement,

velocity, and time, such that the numerical value for the total force acting on any feature can be evaluated based on the instantaneous displacement and velocity of that feature. With these expressions, Lagrange's equation is utilized to derive the full set of equations of motion governing the dynamic behavior of the system. These equations and the defined system initial conditions are then used by the built-in MATLAB ordinary differential equation solver, *ODE15i.m*, to produce a time-domain representation of the system motion throughout the duration of the specified time interval. This solution provides a wealth of information that can serve developers of compliant-moored tidal turbine devices by revealing important details such as the forces experienced by mooring lines and structural features, dynamic resonance characteristics of the system, and predicted device orientation and motion. This also allows major design changes to be evaluated prior to expending the cost for field experimentation.

The validation tests performed thus far provide confidence that the methods employed provide realistic results under limited conditions, but further testing is required to ensure accurate representations of dynamic behavior can be obtained for real-world marine energy devices. Furthermore, the inclusion of additional fluid loading effects such as that from surface waves and turbulence will enhance the utility of this program as a design tool and broaden the scope of systems that can be analyzed. With further development of these techniques for numerically obtaining the dynamic characteristics of a compliant-moored marine energy system, this program has the potential to become an invaluable tool for developers of marine energy technologies.

7. References

- [1] “International Energy Statistics,” U.S. Energy Inf. Adm. [Online]. Available: <http://www.eia.gov/cfapps/ipdbproject/iedindex3.cfm?tid=2&pid=2&aid=12&cid=r3,&syid=2007&eyid=2011&unit=BKWH>. [Accessed: 29-Oct-2013].
- [2] Fraenkel P. L., 2007, “Marine current turbines: pioneering the development of marine kinetic energy converters,” *Proc. Inst. Mech. Eng. Part A J. Power Energy*, **221**(A2), pp. 159–169.
- [3] Delorm T. M., Zappala D., and Tavner P. J., 2011, “Tidal stream device reliability comparison models,” *Proc. Inst. Mech. Eng. Part O J. Risk Reliab.*, **226**(1), pp. 6–17.
- [4] Boehlert G. W., and Gill A. B., 2010, “Environmental and ecological effects of ocean renewable energy development: a current synthesis,” *Oceanography*, **23**(2), pp. 68–81.
- [5] “Tidal Energy Project,” Islay Energy Trust [Online]. Available: <http://islayenergytrust.org.uk/tidal-energy-project/>. [Accessed: 21-Oct-2013].
- [6] MacEnri J., Reed M., and Thiringer T., 2013, “Influence of tidal parameters on SeaGen flicker performance,” *Philos. Trans. R. Soc. A - Math. Phys. Eng. Sci.*, **371**(1985).
- [7] “SeaGeneration (Wales),” Mar. Curr. Turbines Ltd. [Online]. Available: www.seagenwales.co.uk/index.php. [Accessed: 20-Mar-2014].
- [8] “SeaGen S,” Mar. Curr. Turbines Ltd. [Online]. Available: www.marineturbines.com/SeaGen-Products/SeaGen-S. [Accessed: 20-Mar-2014].
- [9] Faez Hassan H., El-Shafie A., and Karim O. a., 2012, “Tidal current turbines glance at the past and look into future prospects in Malaysia,” *Renew. Sustain. Energy Rev.*, **16**(8), pp. 5707–5717.
- [10] Macnaughton D., Fraenkel P. L., Paish O. F., Hunter R., and Derrick A., 1993, “Tidal stream turbine development,” *Renewable Energy*, pp. 67–71.
- [11] Clarke J., Connor G., Grant A., Johnstone C., and Ordonez-Sanchez S., 2010, “Analysis of a single point tensioned mooring system for station keeping of a contra-rotating marine current turbine,” *IET Renew. Power Gener.*, **4**(6), pp. 473–487.
- [12] “OCGen Power System,” Ocean Renew. Power Co. [Online]. Available: http://www.orpc.co/orpcpowersystem_ocgenpowersystem.aspx. [Accessed: 21-Oct-2013].
- [13] Rhinefrank K., Schacher A., Prudell J., Cruz J., Jorge N., Stillinger C., Naviaux D., Brekken T., von Jouanne A., Newborn D., Yim S., and Cox D., 2010, “Numerical and experimental analysis of a novel wave energy converter,” *International Conference on Ocean, Offshore and Arctic Engineering*, New York, NY, pp. 559–567.

- [14] Hall M., Buckham B., Crawford C., and Nicoll R. S., 2011, "The importance of mooring line model fidelity in floating wind turbine simulations," Oceans, Waikoloa, HI.
- [15] Jonkman J. M., 2013, "NWTC Computer-Aided Engineering Tools," FAST [Online]. Available: <http://wind.nrel.gov/designcodes/simulators/fast/>. [Accessed: 20-Mar-2014].
- [16] Thomson J., Polagye B., Durgesh V., and Richmond M. C., 2012, "Measurements of Turbulence at Two Tidal Energy Sites in Puget Sound, WA," IEEE J. Ocean. Eng., **37**(3), pp. 363–374.
- [17] Thomson J., Kilcher L., Richmond M., Talbert J., DeKlerk A., Polagye B., Guerra M., and Cienfuegos R., 2013, "Tidal turbulence spectra from a compliant mooring," Marine Energy Technology Symposium, Washington, D.C.
- [18] Kelly N. D., and Jonkman J. M., 2007, Overview of the TurbSim stochastic inflow turbulence simulator.
- [19] Vicente P. C., Falcão A. F. deO., Gato L. M. C., and Justino P. A. P., 2009, "Dynamics of arrays of floating point-absorber wave energy converters with inter-body and bottom slack-mooring connections," Appl. Ocean Res., **31**(4), pp. 267–281.
- [20] Jonkman J. M., 2009, "Dynamics of offshore floating wind turbines: Model development and verification," Wind Energy, **12**(5), pp. 459–492.
- [21] Morison J. R., O'Brien M. P., Johnson J. W., and Schaaf S. A., 1950, "The force exerted by surface waves on piles," Trans. Am. Inst. Min. Metall. Eng., **189**, pp. 149–154.
- [22] Gabbai R. D., and Benaroya H., 2005, "An overview of modeling and experiments of vortex-induced vibration of circular cylinders," J. Sound Vib., **282**(3-5), pp. 575–616.
- [23] Parkinson G., 1989, "Phenomena and modelling of flow-induced vibrations of bluff bodies," Prog. Aerosp. Sci., **26**, pp. 169–224.
- [24] Irvine M., 1992, Cable Structures, Dover Publications.
- [25] Raman-Nair W., and Baddour R. E., 2002, "Three-dimensional coupled dynamics of a buoy and multiple mooring lines: Formulation and algorithm," Q. J. Mech. Appl. Math., **55**(2), pp. 179–207.
- [26] DuBuque G., 2011, "A Lumped Parameter Equilibrium Model of a Submerged Body with Mooring Lines," University of Washington.
- [27] Dewhurst T., Swift M. R., Wosnik M., Baldwin K., DeCew J., and Rowell M., 2013, "Dynamics of a floating platform mounting a hydrokinetic turbine," Mar. Technol. Soc. J., **47**(4), pp. 45–56.

Appendix A. How to use UWMooringDynamics.m

A system can be configured either through a dialog in the MATLAB Command Window or as a saved *m*-file. Upon execution, the user is prompted to state whether a new system will be assembled or if a saved configuration file will be loaded. In either case, the same commands are used to build the system, the only difference being whether they are entered manually in sequence or called in a script. A model is constructed by setting the general system parameters, including the fluid flow characteristics, and then adding device features one-by-one by invoking the *newBody.m*, *newNode.m*, and *newline.m* commands. All quantities are treated as having measurements consistent with the International System of Units (length expressed as meters, mass expressed as kilograms, etc.).

A.1. Setting General System Parameters

Once the program is executed, the first step in constructing a system model is to modify the general system parameters. These parameters are the fluid velocity components (typically expressed as functions of space and time), fluid density, simulation time interval, acceleration due to gravity, and the domain and perspective of the output animation. The default values for these parameters are given in Table 4.

Table 4: Default values for general system parameters

Property	Variable Name	Default Value	Units
Free Stream Velocity	Ux	0	m/s
	Uy	0	
	Uz	0	
Fluid Density	rho_f	1020	kg/m^3
Time Span	t0	0	s
	tf	30	
	tStep	0.1	
Gravitational Accel.	grav	9.81	m/s^2
Domain	domain	$[x_{min} \ x_{max} \ y_{min} \ y_{max} \ z_{min}]$ = [-10 10 -10 10 0 20]	m
Perspective	perspective	$[Azimuth \ Elevation]$ = [105 10]	$degrees$

A parameter is modified to match a given physical system by changing the value assigned to the corresponding variable, either in the MATLAB command window if the system is being constructed manually, or in the system configuration script file of a saved system. Note that the variables `domain` and `perspective` are stored as a 1x6 and 1x2 row vector, respectively, with each entry corresponding to the associated parameter as listed in Table 4.

The free stream velocity is defined by its component magnitudes in the inertial coordinate directions. Each component can be any function of space and time using the variables x , y , z , and t . For example, the following command defines the free stream velocity in the inertial y -direction as a function of height above the seafloor (z) and periodic in time with a period of 60 seconds:

$$U_y = z^{(1/7)} * \sin(\pi * t / 30);$$

The variables `t0` and `tf` correspond to the start time and end time of the simulation, and therefore define the time interval over which the differential equations of motion are solved. The variable `tStep`

defines the temporal resolution of the solution output; that is, the solution will give the value for each independent displacement variable every `tStep` seconds within the time interval. `tStep` is not used by the ODE solver as a time step for the numerical integration; changing its value only affects the number of temporal data points in the solution, but not the accuracy of the solution. The variables `domain` and `perspective` only pertain to the solution output animation, which provides a visual representation of the dynamic behavior of the system. The former defines the bounds for each axis displayed in the animation, while the latter identifies the viewing angle. With the value of `perspective` set to `[0 0]`, the output animation will be seen looking along the positive y -axis, with the x -axis positive to the right and the z -axis positive in the upwards direction. The first entry in `perspective` identifies the rotation of the viewing angle about the vertical z -axis (azimuth), and the second entry indicates the angle up from the horizontal (elevation), both expressed in degrees. The default domain of `[-10 10 -10 10 0 20]` and `perspective` of `[105 10]` displays the animation in the space shown in Figure 27.

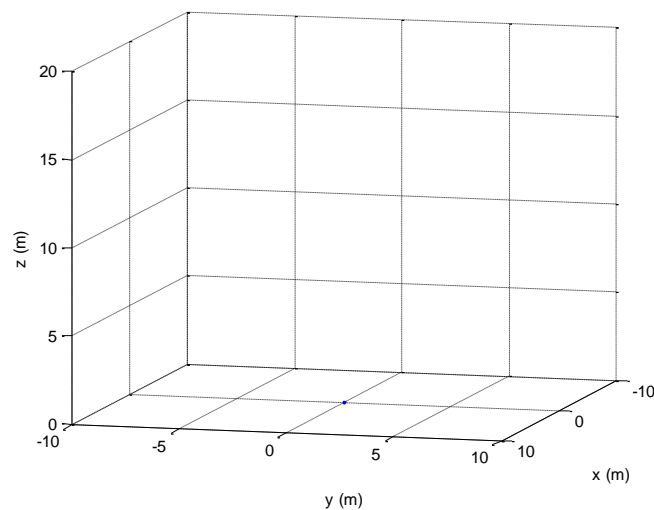


Figure 27: Default animation space and viewing angle

The values for `domain` and `perspective` can also be modified after the solution is obtained and the animation can be replayed with the new values with a manual call to the `Animate.m` function.

With the general parameters appropriately defined, system features can now be added using the `newBody`, `newNode`, and `newLine` commands.

A.2. Adding Rigid Bodies

A call to the `newBody` function adds a rigid body to the system. Table 5 lists all properties associated with a rigid body and their default values.

Table 5: Parameters and default values associated with rigid bodies

Property	Property Name	Default Value
Name	Name	“Body#” where # is replaced by the numerical body identifier
Mass	Mass	$m = 1 \text{ kg}$
Mass Moment of Inertia	MMoI	$I = [I_x \ I_y \ I_z]^T$ $= [1 \ 1 \ 1]^T \text{ kg m}^2$
Added Mass	AddedMass	$m_{added} = 0$
Volume	Vol	$V = 2 \text{ m}^3$
Initial Position	InitPosition	${}^0\vec{P}_0 = [x_0 \ y_0 \ z_0] = [0 \ 0 \ 0]^T$
Initial Orientation	InitOrientation	$[\alpha_0 \ \beta_0 \ \gamma_0] = [0 \ 0 \ 0]^T$
Initial Velocity	InitVelocity	${}^0\vec{V}_0 = [0 \ 0 \ 0]^T$
Initial Angular Velocity	InitAngularVelocity	${}^0\vec{\omega}_0 = [0 \ 0 \ 0]^T$
Applied Forces, Global Frame	AppliedForcesGlobal	${}^0\vec{F}_{app} = [0 \ 0 \ 0]^T$
Applied Moments, Global Frame	AppliedMomentsGlobal	${}^0\vec{M}_{app} = [0 \ 0 \ 0]^T$
Applied Forces, Body-Fixed Frame	AppliedForcesBodyFixed	${}^i\vec{F}_{app} = [0 \ 0 \ 0]^T$
Drag	AppliedMomentsBodyFixed	${}^i\vec{M}_{app} = [0 \ 0 \ 0]^T$

Property	Property Name	Default Value
Axis-Aligned Characteristic Area	Area	$[A_x \ A_y \ A_z] = [1 \ 1 \ 1]^T$
Translational Damping	TransDissipation	$b_{trans} = 0$
Angular Damping	AngularDissipation	$b_{rot} = 0$
Representative Dimensions	Dims	$[L_x \ L_y \ L_z] = [2 \ 2 \ 2]^T$
Fixed Frame	FixedFrame	0 (free body)

At the time the *newBody* function is called, the user may change any of the values listed in Table 5 to match the physical properties of the body being modeled. This function uses a variable-length input argument list, therefore any parameter that is not being changed does not have to be explicitly addressed in the function call. To change a parameter value, the user enters a parameter-value pair into the function argument list with the name of the parameter being changed (as a character string), followed by the value to which it is being changed. The order in which parameter-value pairs are entered in the argument list is of no consequence. Any parameter that is stored as an array is entered as a column vector following MATLAB syntax. For example, to add a body to the system with a mass of 200 kg, an initial position at coordinates (2,4,6) m in the inertial frame, and all other parameters set to default values, the following command is entered:

```
newBody('Mass',200,'InitPosition',[2;4;6])
```

The mass moment of inertia is defined about the body-fixed axes originating from the center of mass of the body and can usually be calculated from the mass and physical dimensions of bodies with simple geometries. If the initial orientation of the rigid body is left at its default value of [0;0;0], then its body-fixed coordinate axes initially are parallel to the corresponding inertial axis.

The volume of a body is used only to calculate the force of buoyancy to which the body is subjected following the methods described in Section 3.8.2. Alternatively, if the buoyant force on a body is already known but the volume is not readily available, the buoyant force can be entered as an applied force and the body's volume can be set to zero without need for further system or code modification. Applied forces and moments can be defined with respect to the global frame or the body-fixed frame. Forces defined in the global frame describe forces whose direction of action does not depend on the orientation of the body. Conversely, a force defined in the body-fixed frame acts in a direction that is dependent on the orientation of the body with respect to the inertial frame. Application of forces defined in the body-fixed frame are useful for modeling mechanisms such as thrust generated by a body or the reactive torque experienced by most tidal turbines.

The axis-aligned characteristic area of a body is used in the calculation of the fluid drag force, as described in Section 3.8.3.1. The translational and angular damping coefficients are independent of viscous damping and are used to apply additional linear damping terms to the system. The representative dimensions of a body are used to define the dimensions of the box drawn to represent that body in the animation of the system dynamics and have no impact on the governing equations of motion. The first entry corresponds to the length of the body along its body-fixed x -axis, the second entry to the length along the y -axis, and the third entry corresponds to the z -axis.

A new body can be constrained to a fixed position in the coordinate frame of an existing body by modifying the 'fixed frame' parameter. A new body is fixed to an existing body by changing the value of 'FixedFrame' to the name of the body to which it is to be constrained. For example, to fix a new body to an existing body named 'Body2', the argument pair (*FixedFrame*, 'Body2') is included in the argument list passed to the *newBody* function. When a new body is fixed to another body, the parameter 'InitPosition' defines the coordinates of the center of mass of the constrained body within the parent body-fixed frame. That is, passing the argument list (*FixedFrame*, 'Body2',

'*InitPosition*', [0; 2; -1]) to the *newBody* function will fix the new body to the coordinate position (0, 2, -1) in the body-fixed frame belonging to the Body2.

For a free body, i.e. a body unconstrained to any other body in the system, the variable 'InitPosition' describes the coordinates of the origin of the body with respect to the inertial frame.

A.3. Adding Free Nodes

A free node is used in situations where multiple lines are joined at junctions characterized by small geometries and mass, such that it is not necessary to represent the joining structure as a rigid body. Two or more lines joined with a shackle, small swivel, or other types of links are best modeled as lines terminating at a common free node, rather than a rigid body. This opens up a greater range of possibilities for mooring line configurations, as it can connect lines of differing materials together to form sophisticated cable structures. A free node is added with a call to the *newNode* function. The only parameters associated with a free node are its name, mass (defaulted to zero), and initial position (defaulted to the origin of the inertial frame). Like the *newBody* function, when *newNode* is called a node is added to the system with default parameter values, unless those values are changed by passing an argument list to the *newNode* function containing parameter-value pairs for each parameter being changed.

A.4. Adding Mooring Lines

The *newline* function is called upon to form the connections between rigid bodies, free nodes, and the seafloor. The parameters associated with each new mooring line and their default values are given in Table 6.

Table 6: Parameters and default values associated with mooring lines

Property	Property Name	Default Value
Name	Name	"Line#" where # is replaced by the actual number of that line
Coordinate frame of start point	StartFrame	0 (inertial frame)
Coordinates of start point	LineStart	${}^0_{LN}\vec{P}_{Start} = [0 \ 0 \ 0]^T$
Coordinate frame of end point	EndFrame	0 (inertial frame)
Coordinates of end point	LineEnd	${}^0_{LN}\vec{P}_{End} = [0 \ 0 \ 0]^T$
Mass per unit length	LinearMass	$m_{Line} = 5 \text{ kg/m}$
Length	Length	$L = 0$ (length will be calculated by program)
Diameter	Diameter	$d = 0.05 \text{ m}$
Spring stiffness of one meter of line	UnitK	$k_{Unit} = 1000000 \text{ N m/m}$
Drag coefficient for flow tangential to line axis	TanDrag	$C_{D,Tan} = 0$
Drag coefficient for flow normal to line axis	NormDrag	$C_{D,Norm} = 0$
Number of discretized line segments	NumSegments	$N_{seg} = 8$
Line motion damping constant	DampingCoeff	$b = 0$

The 'StartFrame' and 'EndFrame' parameters define the coordinate frames to which the ends of a mooring line are fixed, and is assigned by indicating the name of the rigid body or free node. If fixed to a rigid body or to the inertial frame, the 'LineStart' and 'LineEnd' parameters define the coordinates of the corresponding line terminus with respect to the coordinate frame to which it is fixed. If the line

terminus is fixed to a free node, 'LineStart' and 'LineEnd' are disregarded. Mass is given to the lines as a uniform quantity per unit length, and can be defined by modifying the 'Length' parameter. If this parameter is left as its default value of zero, the line length will be calculated from the given system geometry as the length of the vector from the line start point to its end point. The diameter of a mooring line is used in the calculation of the fluid drag forces acting on a line segment, as described in Section 3.8.3.1.

The spring stiffness of a line is stated as a quantity for a unit length. In this way, simulations can be conducted with varying line lengths without needing to re-calculate the resulting stiffness each time a new line length is evaluated. The unit-length stiffness of a particular line material can be determined if the stiffness of a given length of line is known by $k_{unit} = k/L$. The drag coefficients can be determined experimentally, as well as computationally or theoretically by treating the line as a cylinder. The tangential drag coefficient corresponds to axial flow and the normal drag coefficient corresponds to flow perpendicular to the axis of the line segment.

A.5. Example: DuBuque System

The test system presented in Section 4.1.3 is modeled with a single rigid body anchored by four mooring lines submerged in a constant fluid flow of 4 m/s. The initial position of the rigid body is chosen such that the origin of its body-fixed coordinate frame is centered above the origin of the inertial x - y -plane at a height of 20 m above the seafloor. The four mooring lines, following the schematic shown in Figure 18, are anchored to the seafloor at coordinates (35, -30, 0), (35, 30, 0), (-35, 30, 0), and (-35, -30, 0) in the inertial frame with units of meters. The mooring lines are attached to the rigid body at the body-fixed coordinates (7, -2, 0), (7, 2, 0), (-7, 2, 0), and (-7, -2, 0). All other parameters required to model this system are given in Table 1 and Table 2.

To begin the simulation from the MATLAB command window, the path must first be set to the folder containing the program m-files. The main program file is titled *UWMooringDynamics.m*, therefore the program is executed by entering the command `UWMooringDynamics` in the MATLAB command window. The following prompt will appear:

```
Enter "new" to build a new system or  
"load" to load an existing system
```

Since this system is saved as a configuration m-file, the user enters `load` and is then prompted to provide the name of the m-file where the system configuration is saved:

```
Enter filename of system you wish to load
```

The user then types the correct filename. The current system model is saved in an m-file entitled *configDuBuque.m*, therefore the command `configDuBuque` is entered to load this system. The user then has the option to add additional features (lines, nodes, or bodies) to the system or to run it as-is, indicated by the prompt:

```
Enter "run" to begin the simulation or  
"add" to include additional features
```

Since no additional features are required for this simulation, the user types 'run' in the command window to tell the program to begin deriving the equations of motion based on the given system information.

The system is saved as a script. The first lines of the script file are used to define the fluid velocity components and other general system properties as described above. The only general parameters for this system that differ from the default values are the y-component of fluid velocity and the domain of the output animation. The first two lines of the system file *configDuBuque.m* are therefore:

```

Uy = 4;
domain = [-35, 35, -35, 35, -20, 50];

```

The domain was chosen to enclose the whole system while maintaining a 1:1 aspect ratio between the coordinate axes. Next, the rigid body is inserted with a call to the *newBody.m* function, using parameter-value pairs as the function argument to define the appropriate body properties as detailed in Section 4.1.3:

```

newBody('Name','Turbine','Mass',5000,'MMoInertia',[4;4;4],
        'Vol',10,'InitPosition',[0;0;20],'Drag',[0.5;0.5;0.5],
        'Area',[16;24;11],'Dimensions',[28;4;8.5]);

```

The four mooring lines are now added using the *newLine.m* function with parameter-value pairs that match the line properties described in Section 4.1.3 and the selected coordinate frame described above.

The *newLine.m* function is invoked once for each line:

```

newLine('Name','LineBottomLeft','LineStart',[35;-30;0],
        'EndFrame','Turbine','LineEnd',[7;-
2;0],'LinearMass',10,
        'Length',44,'Diameter',0.05,'UnitK',19635000,
        'TangentialDrag',0.3,'NormalDrag',1,'NumSegments',8);

newLine('Name','LineBottomRight','LineStart',[35;30;0],
        'EndFrame','Turbine','LineEnd',[7;2;0],'LinearMass',10,
        'Length',44,'Diameter',0.05,'UnitK',19635000,
        'TangentialDrag',0.3,'NormalDrag',1,'NumSegments',8);

newLine('Name','LineTopRight','LineStart',[-35;30;0],
        'EndFrame','Turbine','LineEnd',[-
7;2;0],'LinearMass',10,
        'Length',44,'Diameter',0.05,'UnitK',19635000,
        'TangentialDrag',0.3,'NormalDrag',1,'NumSegments',8);

```

```

newLine('Name','LineTopLeft','LineStart',[-35;-30;0],
        'EndFrame','Turbine','LineEnd',[-7;-
2;0],'LinearMass',10,
        'Length',44,'Diameter',0.05,'UnitK',19635000,
        'TangentialDrag',0.3,'NormalDrag',1,'NumSegments',8);

```

With this, the system described in Section 4.1.3 is fully configured for modeling by the

UWMooringDynamics.m program.

Once the program finishes its computations, the solution is given in a matrix saved to the MATLAB workspace as the variable *Y*. Each column of this matrix corresponds to an independent displacement variable, while each row corresponds to a time, with the first row giving the values of each displacement variable at time *t0* and the last row giving them at time *tf*, and every row in between giving the position of each variable in time increments of *tStep*. A column vector called *Time* is also stored in the workspace, which gives the time in seconds corresponding to the columns in the displacement matrix *Y*. This information can be used to find the tension in each individual line segment, the forces on the mooring line attachment points of the rigid bodies, instantaneous velocities of the bodies, and other characteristics of the dynamic response of the system to the input fluid velocity.

Appendix B. UWMooringDynamics program files

The MATLAB files developed run the dynamic mooring simulation presented in this paper are available online at:

<http://abs-5.me.washington.edu/pub/uwmooring/>